AMERICAN UNIVERSITY OF BEIRUT

PREPARATION AND IN-VITRO CYTOTOXICITY EVALUATION OF RUTHENIUM POLYPYRIDYL-SENSITIZED PARAMAGNETIC TITANIA NANOPARTICLES FOR PHOTODYNAMIC THERAPY

by
MOHAMAD HASSAN SAKR

A thesis
submitted in partial fulfillment of the requirements
for the degree of Master of Science
to the Department of Chemistry
of the Faculty of Arts and Sciences
at the American University of Beirut

Beirut, Lebanon
April 2015

AMERICAN UNIVERSITY OF BEIRUT

PREPARATION AND IN-VITRO CYTOTOXICITY EVALUATION OF RUTHENIUM POLYPYRIDYL-SENSITIZED PARAMAGNETIC TITANIA NANOPARTICLES FOR PHOTODYNAMIC THERAPY

by

MOHAMAD HASSAN SAKR

Approved by:

Dr. Tarek Ghaddar, Associate Professor — Advisor
Department of Chemistry

Dr. Kamal Bouhadir, Associate Professor — Co-Advisor
Department of Chemistry

Dr. Houssam El-Rassy, Associate Professor — Member of Committee
Department of Chemistry

Date of thesis defense: April 27, 2015

AMERICAN UNIVERSITY OF BEIRUT

THESIS, DISSERTATION, PROJECT RELEASE FORM

Student Name: _____
Last First Middle

○ Master's Thesis ○ Master's Project ○ Doctoral Dissertation

☐ I authorize the American University of Beirut to: (a) reproduce hard or electronic copies of my thesis, dissertation, or project; (b) include such copies in the archives and digital repositories of the University; and (c) make freely available such copies to third parties for research or educational purposes.

☐ I authorize the American University of Beirut, **three years after the date of submitting my thesis, dissertation, or project,** to: (a) reproduce hard or electronic copies of it; (b) include such copies in the archives and digital repositories of the University; and (c) make freely available such copies to third parties for research or educational purposes.

_____

Signature Date

ACKNOWLEDGEMENTS

My special and sincere gratitude to Dr. Tarek Ghaddar for his valued guidance and supervision, and my recognition to the committee members. Special thanks to Dr. Marwan El-Sabban for his cooperation in accomplishing this project. The financial support of this work by the Farouk Jaber Research foundation is gratefully acknowledged.

AN ABSTRACT OF THE THESIS OF

Mohamad Hassan Sakr for Master of Science
Major: Chemistry

Title: Preparation and in-vitro cytotoxicity evaluation of ruthenium polypyridyl-sensitized paramagnetic titania nanoparticles for photodynamic therapy

Core-shell-shell magnetite-silica-titania nanoparticles (Fe_3O_4@SiO_2@TiO_2 NPs) were synthesized by successive sol-gel methods. The magnetite cores were electrostatically stabilized and dispersed by the addition of polyacrylic acid. Infrared, energy-dispersive X-ray and X-Ray diffraction measurements of the multilayered NPs confirmed the presence of the surfactant polymer and the three oxides. The surface area, measured by nitrogen adsorption, increased following every step of the synthesis from 95 m^2/g to 233 m^2/g. The intensity-weighted mean diameter of the TiO_2 coated sample was measured by dynamic light scattering and found to be 98.8 nm. Following hydrothermal treatment of the final nanocomposites, a ruthenium polypyridyl dye was anchored to their surface. The total reactive oxygen species (ROS) generation and singlet oxygen production by the obtained hybrid NPs (naked NPs + Ru-dye) were evaluated by fluorescence and UV-Vis spectroscopy in solution. Using a green light (532 nm) for excitation, the total ROS generated by the hybrid NPs were more than 500% times than those generated by the naked ones, and 550% more than those generated by the ruthenium dye alone. Employing a white light produced similar results. As for singlet oxygen generation, the hybrid NPs produced negligible amounts. These findings demonstrate that our hybrid NPs can potentially act as type I photodynamic therapy (PDT) agents generating free radicals, unlike the currently employed ones in medicine which follow type II mechanism predominantly (generating singlet oxygen). This type of photosensitizers can prove advantageous in fighting PDT-resilient hypoxic tumors, and avoiding type II photosensitizers-induced hypoxia in non-hypoxic tumor cells.

CONTENTS

ILLUSTRATIONS

Figure Page

TABLES

Table Page

CHAPTER 1

PHOTODYNAMIC THERAPY

1.1 Definition and Mechanisms of Action

The term photodynamic therapy (PDT) as applied to biomedical science and, more particularly, to clinical medicine is generally defined as the use of a compound or drug (photosensitizer) that has no or minimal effect alone but which, when activated by light, generates one or more reactive chemical species that are able to modify or kill cells and tissues [1]. Its advantages include cost effectiveness, highly localized treatments, sparing of extracellular matrix that allows regeneration of normal tissue, repetition of therapy without accumulation of toxicity, possibility of combining with chemotherapy, which leads to higher cure rates, and induction of immunity, which may contribute to long-term tumor control and suitability for outpatient therapy [2].

Depending on the part of the body being treated, the photosensitizer is administered by intravenous injection or local application. Light is applied to the area to be treated after the drug has been absorbed by the pathologic tissue. The photosensitizer activated by light forms reactive oxygen species (ROS) that kill the cancer cells directly by way of type I and/or type II reactions. Type I reaction involves the production of radicals resulting from the activated sensitizer reacting with plasma membrane or other intracellular molecules. Type II reaction involves generation of singlet oxygen ($^1O_2$) upon energy transfer from the activated sensitizer to oxygen. PDT may also work by destroying tumor-associated vasculature, leading to tumor infarction or by alerting the immune system to attack the cancer. Responses to photodynamic treatment are dependent on the type of photosensitizer used, its extracellular and intracellular localization, the total dose administered, the total light exposure dose, light fluence rate, the

time between the administration of the drug and light exposure, the oxygenation status of the tissue, and the type of cells involved [3].

Cancer cells respond to photodynamic damage by eliciting a rescue response and/ or by undergoing cell death. Rescue responses often involve changes in gene and protein expression of stress proteins, allowing the cells to cope with the damage. PDT may result in cell death via apoptosis, necrosis, or autophagy, which can be affected by the cell type, the nature of photosensitizers, the incubation protocol, and the light dose [4, 5]. The physical and chemical natures of the photosensitizers, such as hydrophobicity and charge, are of great importance in determining their subcellular localization. The sensitivity of intracellular components to photo-oxidation via photodynamic action plays an important role in photo-cytotoxicity. Photosensitizers can localize in mitochondria, lysosomes, endoplasmic reticulum, Golgi apparatus, and plasma membranes, which leads to different signaling pathways involved in cell death [6].

The essential goal of PDT is to induce efficient damage to tumor tissue while sparing the surrounding tissue. A selective therapeutic effect of PDT is achieved from preferential accumulation of photosensitizers and from irradiation of the target tissue. Some photosensitizers can reach higher concentrations in tumor tissue than in surrounding healthy tissue due to the abnormal physiology of tumors, such as poor lymphatic drainage, leaky vasculature, decreased pH, increased number of receptors for low-density lipoprotein, and abnormal stromal composition [7].

1.2 Photosensitizers

A large number of photosensitizers have been tested in vivo and in vitro in PDT experiments, but very few have shown ideal properties; for this reason, recent studies have focused on the development and efficacy of new photosensitizers [8]. The prerequisites for an

ideal sensitizer include chemical purity, selectivity for tumoral cells, chemical and physical stability, short time interval between administration and maximal accumulation within tumor tissues, activation at wavelengths with optimal tissue penetration and rapid clearance from the body [9]. The four main classes of photosensitizers are porphyrin derivatives, chlorins, and phtalocyanines which all exhibit different photochemical and photophysical properties in terms of mechanisms of action and light activation [8].

1.2.1 Photophysics and Photochemistry

For all the photosensitizers in current clinical use and with many of those under development, the primary photophysical process involved is believed to be the generation of singlet oxygen, $^1O_2$, by the process illustrated in Figure 1. In this so-called Type II reaction, the singlet oxygen is produced from ground-state oxygen ($^3O_2$) that is present in the target cells or tissues which gets excited by energy exchange from the triplet state (T_1) of the photosensitizer. This triplet state is generated from the singlet state (S_1) that is formed by absorption of a photon of light by the ground-state photosensitizer molecule (S_0). In this process, the S_0 state of the photosensitizer is regenerated, so that the cycle is complete: typically, this may occur many thousands times for a given molecule during a PDT treatment, so that in effect the photosensitizer serves as a catalyst in the conversion of light energy. The $^1O_2$ molecule is responsible then for chemical alterations in target biomolecules in the cells/tissue, resulting in one or more of the various biological effects. For maximum efficacy, the quantum efficiency of the photosensitizer should be high, i.e., the probability that a molecule of $^1O_2$ will be generated following absorption of a photon by the photosensitizer ground state, should be close to 100%. It is the fact that the ground state of oxygen ($^3O_2$) is a triplet state, making the $T_1 \rightarrow {}^3O_2$ transition quantum-mechanically allowed (no change of spin), that allows photosensitizers to have usefully high $^1O_2$ quantum yields [1].

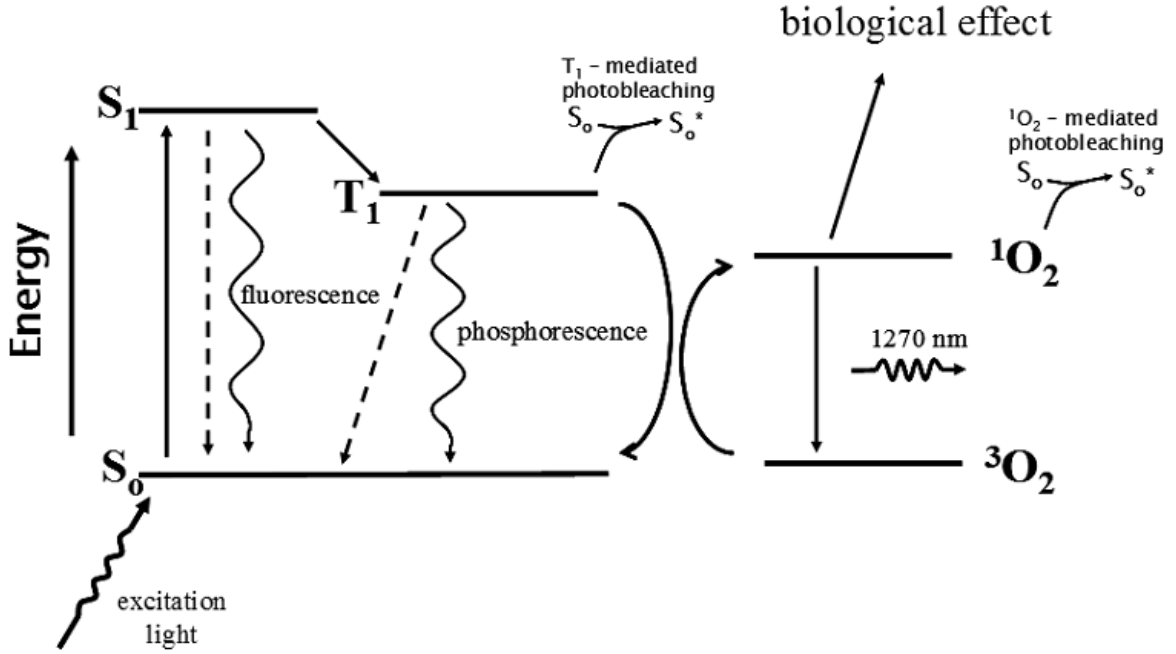

Figure 1: Jablonski energy diagram for Type II photophysics, showing absorption of a photon by the molecular ground state (S_0), raising it to an excited singlet state (S_1), from where it may i) undergo intersystem crossing to the triplet state (T_1), ii) decay radiatively, emitting a fluorescence photon or iii) de-excite nonradiatively (dashed line). The T_1 state can then either decay back to S_0 by phosphorescence emission, or can exchange energy with ground-state oxygen ($^3O_2$) to generate the excited singlet oxygen state ($^1O_2$). $^1O_2$ may then cause biochemical changes with nearby molecules in the cells or tissue or may decay radiatively to $^3O_2$, emitting a near-infrared photon. Two photo-bleaching pathways are also indicated [1].

The energy gap between the excited and ground-state oxygen molecules is close to 1 eV, so that this would be the minimum photon energy required to trigger the Type-II reaction. In practice, the efficiency of $^1O_2$ production is limited to photon energies above 1.5 eV, corresponding to wavelengths below about 800 nm. In the alternative, Type I reaction, the chemical changes in the biomolecules (which are generally different from those in Type II reactions, although the "downstream" biological effects may be similar), are caused by interactions of either the excited singlet (S_1) or triplet (T_1) states themselves, without the oxygen intermediary [1].

Table 1 lists the series of reactions that occur during PDT. PS is the photosensitizer, ^{1}PS is PS in ground state, ^{1}PS* and ^{3}PS* are PS in singlet excited and triplet excited states, respectively, and D is an electron donor molecule, e.g., NADH (nicotinamide adenine dinucleotide), cysteine, etc. The reaction between ^{3}PS* and ^{1}PS leads to PS anion and cation

radicals, $PS^{-\bullet}$ and $PS^{+\bullet}$, respectively. D can react with $^3PS^*$ to produce more $PS^{-\bullet}$ and oxidized donor (D^+). The superoxide anion, $O_2^{-\bullet}$, is shown to form via two routes: (1) $PS^{-\bullet}$ electron exchange with oxygen and (2) electron transfer of $^3PS^*$ with oxygen. $O_2^{-\bullet}$ formation from $^3PS^*$, however, competes with the production of singlet oxygen (type II). Also, two superoxide anion molecules can combine with protons to produce hydrogen peroxide. The subsequent steps include reduction of Fe^{3+} by $O_2^{-\bullet}$, and Fe^{2+} reaction with hydrogen peroxide to form a hydroxyl radical. This species can interfere with the biological functions of nucleic acids, fatty acids, and certain amino acids [10]. Type II process involves only a limited number of molecules because the reacting species must have triplet state multiplicity [11]. Type I and Type II processes can occur at the same time; however, Type II is the dominant process in PDT and it is a catalytic process [10].

Table 1: Reactions occurring during photodynamic action [10].

Excitation	$^1PS + h\nu \rightarrow {}^1PS^* \rightarrow {}^3PS^*$		
Photoprocess	**Reaction**		**Product**
Type I	$^3PS^* + {}^1PS$	$\rightarrow$	$PS^{-\bullet} + PS^{+\bullet}$
	$^3PS^* + D$	$\rightarrow$	$PS^{-\bullet} + D^+$
	$PS^{-\bullet} + O_2$	$\rightarrow$	$^1PS + O_2^{-\bullet}$
	$^3PS^* + O_2$	$\rightarrow$	$PS^{+\bullet} + O_2^{-\bullet}$
	$2O_2^{-\bullet} + 2H^+$	$\rightarrow$	$O_2 + H_2O_2$
	$Fe^{3+} + O_2^{-\bullet}$	$\rightarrow$	$Fe^{2+} + O_2$
	$Fe^{2+} + H_2O_2$	$\rightarrow$	$O_2 + OH^- + OH^\bullet$
Type II	$^3PS^* + {}^3O_2$	$\rightarrow$	$^1PS + {}^1O_2$

The lifetime of singlet oxygen is very short due to its reactivity. In H_2O, the lifetime is 3.5 μs, in D_2O it is 68 μs [12], in organic solvents its lifetime is 10–100 μs [11], and in lipids it is 50–100 μs [13]. The lifetime decreases dramatically to 0.2 μs inside cells, due to high reactivity with biological substances. Rapid reactivity and a short lifetime limit the

singlet oxygen distribution in cells. Thus, PDT treatments are localized at the point of $^1O_2$ generation and are only about 10 nm in diameter (thickness of a cell membrane) [11, 14].

1.2.2 Main Families

Photosensitizers can be categorized by direct chemical structure and come from several broad families. The first family discovered was based on hematoporphyrin (Hp) and its derivatives, Figure 2. After purification and manipulation hematoporphyrin derivative (HpD) is transformed into commercial products variously called Photofrin®, Photosan, Photocan, etc [15]. These products are composed of differing fractions of porphyrin monomers, dimers, and oligomers which are required for successful therapy [16]. Depending on the purification steps these commercial products may not be identical, though clinically they appear equivalent [17]. Interestingly, with knowledge of the heme synthetic pathway, one can exploit the endogenous photosensitizer protoporphyrin [28]. The prodrug δ-aminolevulinic acid when administered, even topically, will alter the natural heme synthesis feedback loop to create enough excess protoporphyrin for clinical utility [18].

Not to be outdone, nature has given us the magnificent series of chemical events in photosynthesis. Clearly, light energy is well used in this process. Chlorophyll like substances termed chlorines have excellent photosensitizing properties [19]. Multiple drugs have been created with some being commercially available. These include modifications of chlorophyll and chemically synthesized structures. Purins, degradation products of chlorophyll, also are relevant [20]. Certain bacteria and algae have chlorophyll like activity such as the bacteriochlorins [21]. Dyes remain a fertile ground to develop successful photosensitizers. Phtalocyanine dyes appear to have great potential, as do Napthalcyanines [19, 22].

1.2.2.1 Porphyrins

1.2.2.1.1 Hematoporphyrin derivative (HpD)

Photofrin® is commercially available from Axcan Pharma, Inc. and has the longest clinical history and patient track record [18]. The photosensitizer is actually a proprietary combination of monomers, dimers, and oligomers derived from chemical manipulation of hematoporphyrin (Hp) [23]. The latter was produced by Scherer in 1841 by removing iron from blood (Heme) and then treatment with water [24]. HpD was developed by treating Hp with $AcOH/H_2SO_4$ to give a mixture of monomers, dimers, and oligomers, linked by ether, ester, and carbon-carbon bonds [25]. The types of steps associated with its synthesis are illustrated in Figure 2 [26]. Removal of monomers from HpD by heating the reaction mixture in the last step of the synthesis until hydrolysis is complete led to Photofrin®, a product consisting of ether-linked dimers and trimers [17, 24]. Similarly named photosensitizers derived by similar or different means from hematoprophyrins are also available from different groups in different parts of the world [27]. In the US, Photofrin® is FDA approved for early and late endobronchial lesions as well as Barrett's esophagus and esophageal obstructing lesions [28, 29]. Off label use has been extensive as well and is approved worldwide for a number of additional uses.

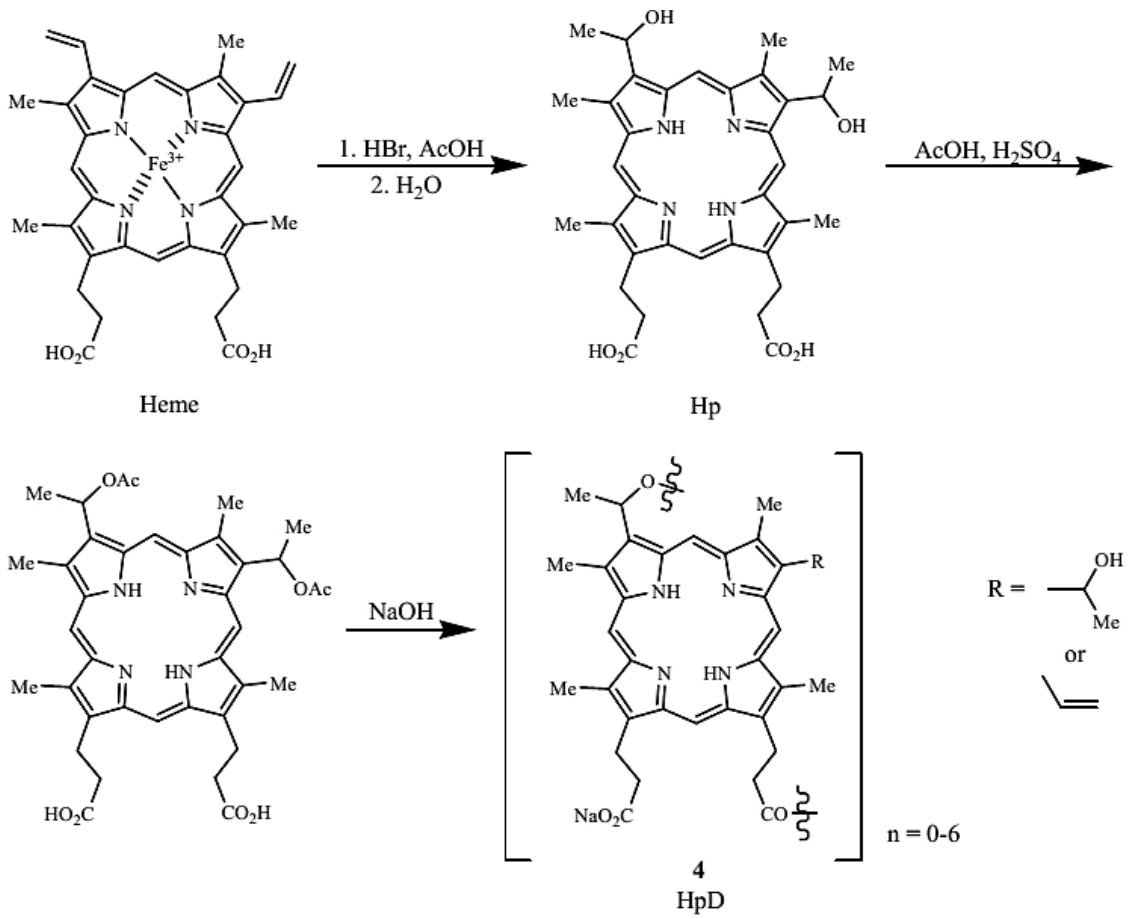

Figure 2: Synthesis of hematoporphyrin derivative (HpD) from heme [10]

Photofrin® and HpD are known as first generation photosensitizers mainly because they exist as complex mixtures of monomeric, dimeric, and oligomeric structures, and the intensity of light absorption at the maximum wavelength (ε_{max}) of Photofrin® is low (ε_{max} at 630 nm ~ 3000 M^{-1} cm^{-1}). This low ε_{max} means that Photofrin® absorbs light weakly at 630 nm. The higher the ε_{max} value the greater the potential photodynamic effect. Also, at 630 nm, the effective tissue penetration of light is small, 2–3 mm, limiting treatment to surface tumors. Its long-term skin phototoxicity lasts six to ten weeks, meaning sunlight and strong artificial light exposure must be avoided during this period. Although Photofrin® has its weaknesses, it gives a high singlet oxygen quantum yield, Φ_{Δ} = 0.89, which indicates efficient generation of $^1O_2$ per photon absorbed. Photofrin® is also safe and was approved in 1993 in Canada for treatment of bladder cancer and in the US FDA for treating esophageal cancer in 1995, lung

cancer in 1998, and Barrett's esophagus in 2003 [30]. Photofrin® treatment extends to head, neck, abdominal, thoracic, brain, intestinal, skin, breast, and cervical cancer [31].

1.2.2.1.2 ALA

5-Aminolevulinic acid (ALA) is a prodrug and a naturally occurring amino acid that is converted enzymatically to protoporphyrin IX (PpIX) [32]. ALA, under trade name Levulan Kerasticks®, was US FDA approved for non-oncological PDT treatment of actinic keratosis in 1999 [33]. Application of ALA prodrug to skin enzymatically transforms it to PpIX photosensitizer via the heme pathway shown in Figure 3. The final step in heme formation by enzyme ferrochelatase is a rate-limiting step, and excess ALA accumulates PpIX in the mitochondria before it slowly transforms into heme [34]. While the PpIX absorption maximum is at 630 to 635 nm, it metabolizes within 48 hours, reducing skin sensitization [35]. Its potential PDT applications extend to Bowen's disease, basal cell carcinoma, and other diseases [36].

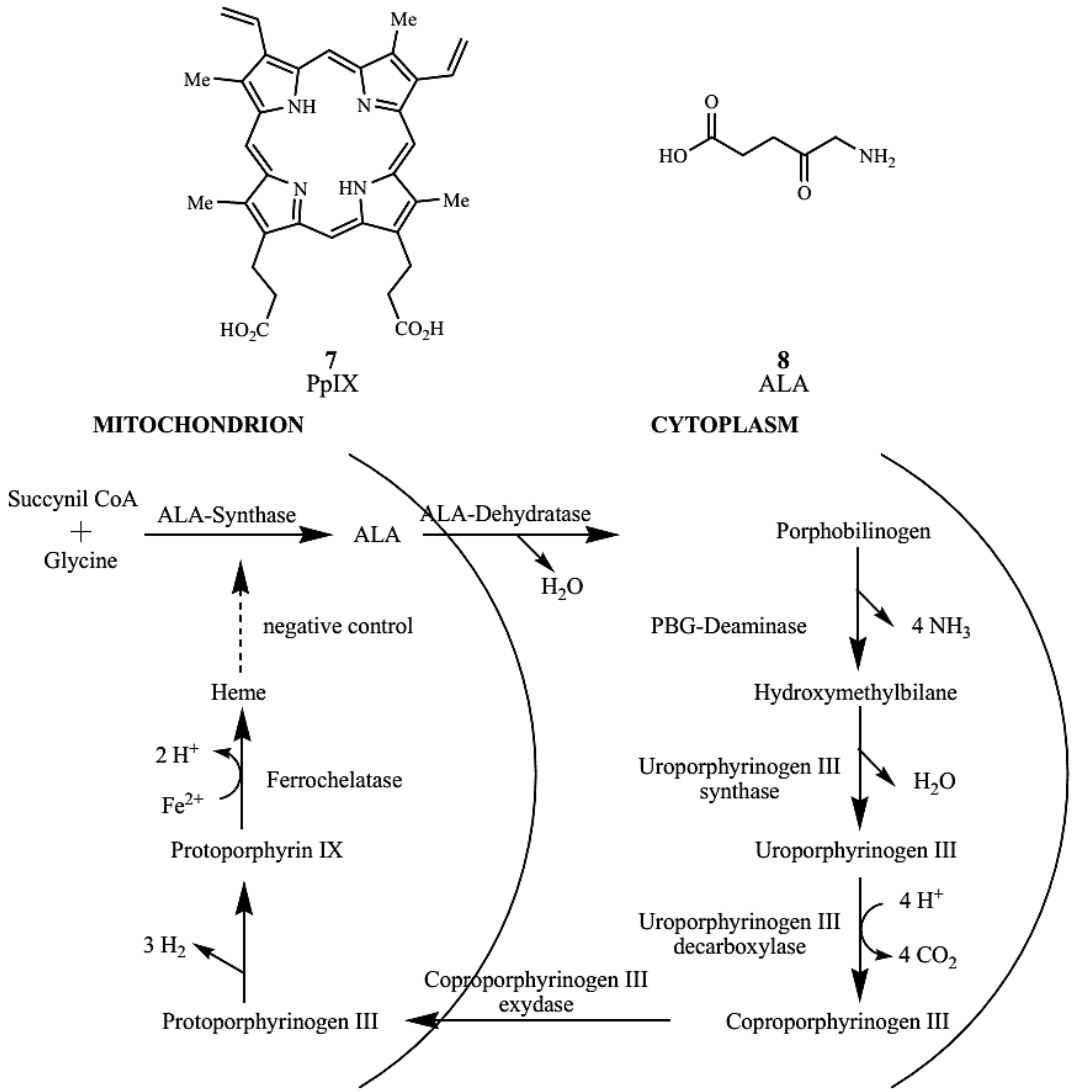

Figure 3: Pathway for heme biosynthesis [10]

The methyl ester of ALA, methyl aminolevulinate (MAL, Metvix®, or Metvixia®; Figure 4), was approved by the US FDA in 2004 for treatment of actinic keratosis. Under the trade name Metvixia®, MAL is also used as a topical treatment and has an advantage over Levulan® due to the nature of the irradiation source. Blu-U® light was approved for use with Levulan® as the most efficient source emitting at 400 nm, while Aktilite® was approved for Metvixia® which emits at 630 nm and provides deeper tissue penetration. MAL is the active component in Visonac® and is being studied for acne vulgaris in Phase II trials (NCT01347879) in the US [10].

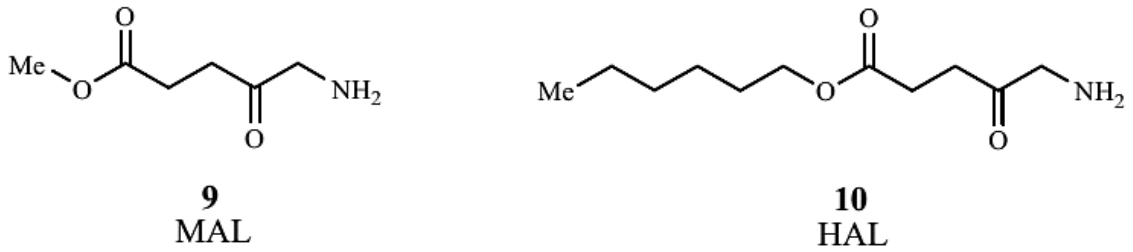

Figure 4: Molecular structures of methyl aminolevulinate (MAL) and Hexaminolevulinate (HAL) [10]

Hexaminolevulinate, the n-hexyl ester of ALA, (HAL, Hexvix®, Cysview®; Figure 4) was approved in 2010 by the US FDA in the diagnosis of bladder cancer. HAL is converted to PpIX 50–100 times more efficiently than ALA [37]. Phase II trials are underway for treatment of cervical intraepithelial neoplasia (NCT01256424), and Phase II/III trials are ongoing for genital erosive lichen planus (NCT01282515).

1.2.2.2 Chlorins

Several photosensitizers evaluated for PDT efficacy are from the chlorin family, Figure 5, and include benzoporphyrin derivative monoacid ring A (BPD-MA, Verteporfin, Visudyne®), meta-tetra(hydroxyphenyl)chlorin (m-THPC, Foscan®), tin ethyl etiopurpurin (SnET2, Rostaporfin, Purlytin™), and N-aspartyl chlorin e6 (NPe6, Talaporfin) which is derived from chlorophyll a. When compared to porphyrins, the structure of chlorins differs by two extra hydrogens in one pyrrole ring. This structural change leads to a bathochromic shift in the absorption band from 640 to 700 nm and gives a ε_{max} ~ 40,000 $M^{-1}cm^{-1}$ [10].

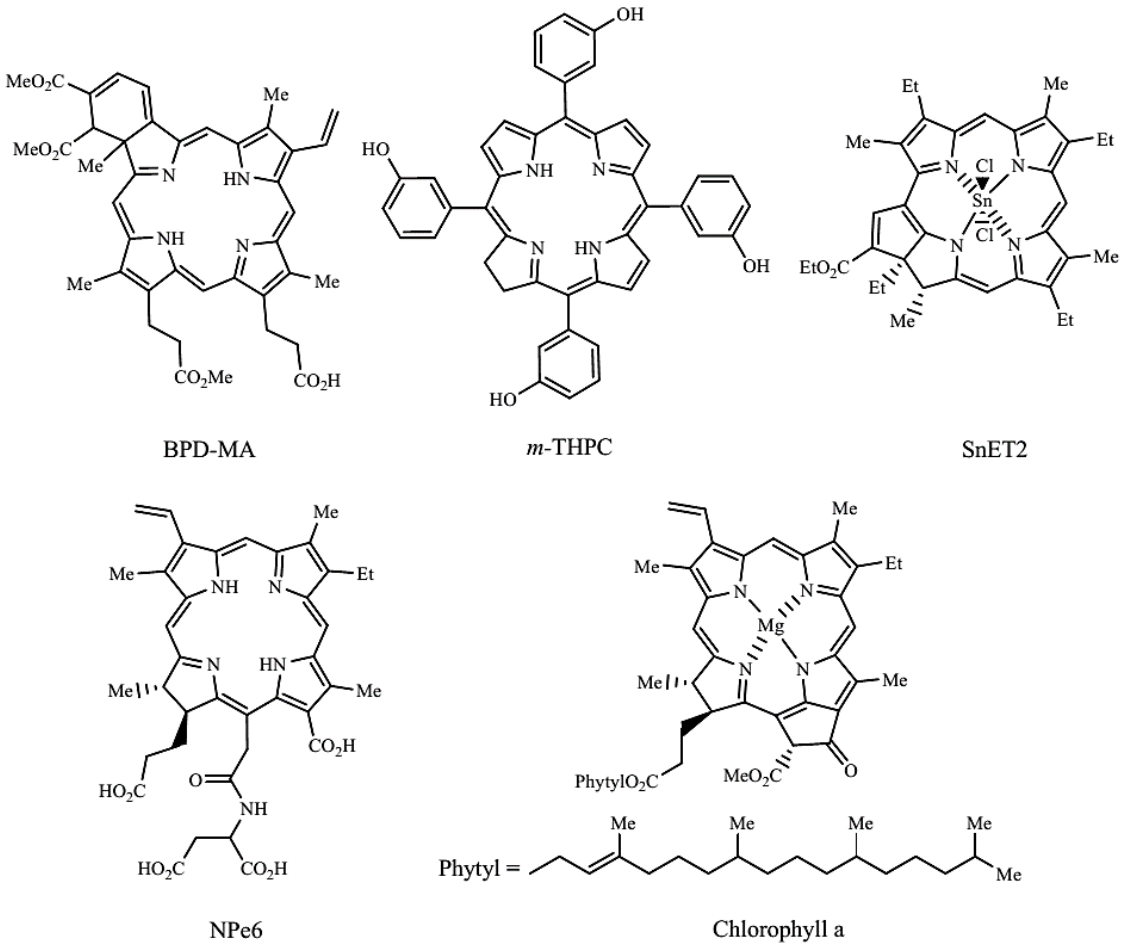

Figure 5: Examples of chlorins evaluated for PDT use [10].

BPD-MA, Figure 5, is activated by light at 689 nm and has a lower time interval of skin phototoxicity than Photofrin®, due to rapid plasma and tissue pharmacokinetics which enables faster excretion of the drug from the body [38]. In 1999, US FDA approved the use of BPD-MA as Visudyne® for age-related macular degeneration in ophthalmology [39]. Additionally, a 24-month study of Verteporfin treatment showed improvement in patients with non-melanoma skin cancer [40].

PDT treatment of neck and scalp cancer with m-THPC was approved in Europe, and the drug was used successfully for treating breast, prostate, and pancreatic cancers [39, 41, 42]. Light activation at 652 nm is very effective and only small doses of m-THPC are required during treatment. A weakness of m-THPC is high skin photosensitivity in some patients.

SnET2, under the trademark Purlytin™, has been evaluated in Phase I/II trials for the treatment of metastatic breast adenocarcinoma, basal cell carcinoma, and Kaposi's sarcoma [43]. This drug has also finished Phase III trials for the treatment of age-related macular degeneration but has not yet been approved by the FDA, due to a requirement of further efficacy and safety assessments. Purlytin™ is activated at 664 nm and has deeper tissue penetration than Photofrin®. The drawback of the drug is a possibility of dark toxicity and skin photosensitivity.

NPe6 is another photosensitizer that can be irradiated at 664 nm for potential PDT treatment of fibrosarcoma, liver, brain, and oral cancer, and was approved in Japan in 2003 to treat lung cancer. Similar to BPD-MA, NPe6 causes minimal skin photosensitivity, unlike Photofrin® [30, 44].

1.2.2.3 Phthalocyanines

Phthalocyanines (Pc) require metal complex formation to exhibit PDT properties since their presence allows the intersystem crossing to occur [45]. Their λ_{max} can be found at 670−700 nm, with ε_{max} ~ 200,000 $M^{-1}cm^{-1}$. One specific Pc derivative is aluminum phthalocyanine tetrasulfonate, AlPcS4, Photosens, (Figure 6) which has a λ_{max} at 676 nm. AlPcS4, as Photosens, has been used in Russia to treat stomach, skin, lip, oral, and breast cancer. However, Photosens produces skin phototoxicity for several weeks [10].

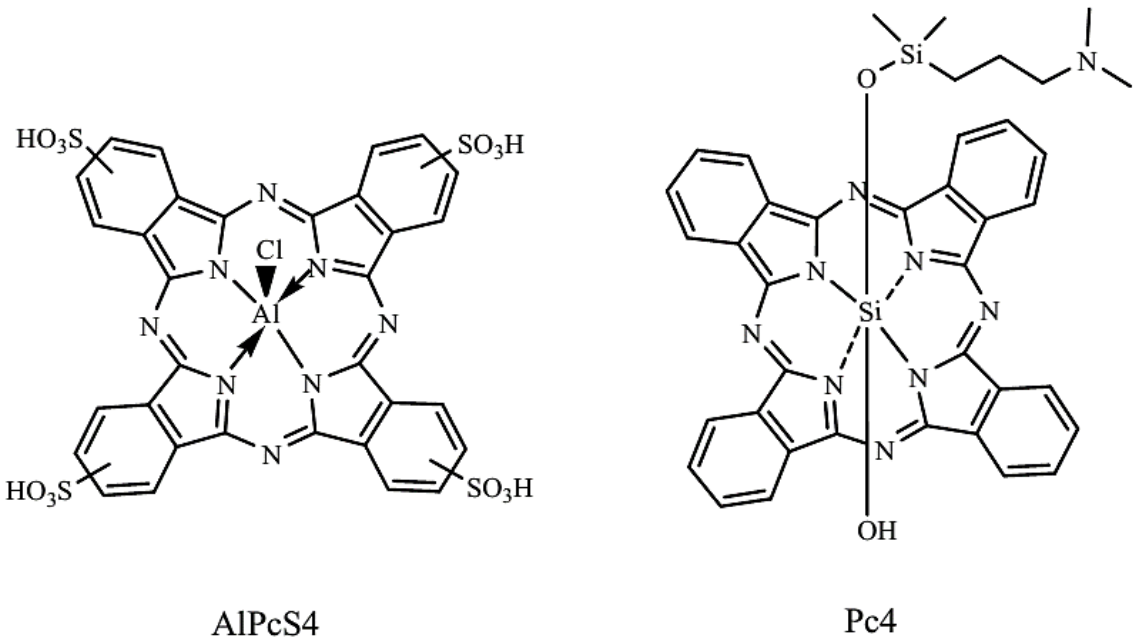

Figure 6: Examples of phthalocyanine PDT sensitizers [45]

Silicon phthalocyanine 4, Pc4, Figure 6, is a phthalocyanine has a maximum absorbance at 675 nm, and it has completed Phase I trials for treating actinic keratosis, Bowen's disease, skin cancer, and State I or II mycosis fungoides [46].

1.3 Ruthenium Polypyridyl Complexes

Ruthenium polypyridyl complexes comprise a versatile class of compounds with unique electrochemical and photophysical properties that have wide applications as oxidation catalysts, photocatalysts, dye sensitizers for solar cells, fabrication of molecular devices, DNA intercalation, and protein binding [47]. Over the last 20–30 years, they have been investigated in perhaps greater detail than any other class of luminescent metal complexes. The extensive synthetic chemistry available allows for systematic manipulation of their physical properties while substituents, which allow immobilization on a variety of surfaces, can be introduced. the investigation of ruthenium polypyridyl complexes exploded in the mid to late 1970's with the realization that the combination of excited state and electrochemical properties of the

compound $[Ru(bpy)_3]^{2+}$ (bpy: bipyridine) should enable it to split water into hydrogen and oxygen [48].

For more than 30 years there has been great interest in the study of the interaction of ruthenium polypyridyl complexes with nucleic acids [49-59]. The anticancer activity of ruthenium complexes is known since decades. NAMI-A and KP1339 are the two most prominent examples of Ru-based anticancer agents since they are currently undergoing clinical trials [52]. Although the targets of ruthenium antitumor complexes have not yet been explicitly established, both NAMI-A and KP1019 can coordinate irreversibly to DNA. Other targets such as plasma proteins and glutathione are also thought to be more important than DNA for their antitumor activities [56]. Another branch in the research of light-activated ruthenium complexes has investigated the ability of such compounds to release ligands and/or undergo ligand exchanges upon light irradiation. For instance, Zayat [60] and Salierno and co-workers [61] have reported complexes that release biologically active molecules upon light irradiation. On the other hand, Sun [62], Goldbach [63], Wachter [64], and Sgambellone et al. [65] have described a series of ruthenium complexes which undergo ligand exchange and subsequent DNA binding or even cleavage upon irradiation at red −NIR wavelengths. Many Ru(II) polypyridyl complexes have been confirmed to possess DNA photocleavage activities through an $^1O_2$ mechanism, thus exhibiting their PDT application potential [66].

The use of ruthenium in PDT, however, has been quite limited so far. There have been multiple reports on porphyrin PSs decorated with ruthenium-based substituents. The resulting hybrid complexes exhibited significantly higher phototoxicity than the individual moieties [67-77]. Charlesworth [78] and Carneiro et al. [79] also investigated organic PSs, phtalocyanines, conjugated to ruthenium moieties. Although the increased PIs are promising, this approach is not ideal as it requires an even longer synthetic pathway than the macrocyclic organic PSs alone. Following a similar approach, Zhou and co-workers coordinated

hypocrellin B, an easily prepared phototoxic compound, to ruthenium. The resulting complex showed promising photosensitizing and photodamage properties in the red −NIR region superior to the hypocrellin B alone [80].

As part of supramolecular systems, ruthenium polypyridyl complexes are rivaled only by porphyrins and metalloporphyrins as active components for photoinduced energy and electron transfer [81]. The luminescence in these compounds originates from a triplet metal-to-ligand charge transfer (^{3}MLCT) excited state, it is possible to tune the related excited-state properties such as the luminescence wavelength, lifetime and quantum yield by tailoring the ligand structure and the rigidity of the complexes. The excitation into either a Franck-Condon ^{1}IL charge transfer band, an appended chromophore via antenna effect, or the ^{1}MLCT absorption band is followed by a rapid intersystem crossing which leads to the population of accessible triplet states. Therefore, one of the initial steps of the relaxation is an ultrafast intersystem crossing (ISC) from the ^{1}MLCT to the lowest-lying ^{3}MLCT excited state in less than 20 fs. A plethora of such complexes have now been synthesized and studied by means of numerous spectroscopic techniques. They have been found to exhibit long luminescence lifetimes due to the triplet character of the emitting lowest ^{3}MLCT excited state; a few nanoseconds to a few milliseconds are possible for Ru(II) complexes [82].

1.4 Nanoparticles in Photodynamic Therapy

The essential goal of PDT is to induce efficient damage to tumor tissue while sparing the surrounding tissue. A selective therapeutic effect of PDT is achieved from preferential accumulation of photosensitizers and from irradiation of the target tissue. Some photosensitizers can reach higher concentrations in tumor tissue than in surrounding healthy tissue due to the abnormal physiology of tumors, such as poor lymphatic drainage, leaky vasculature, decreased pH, increased number of receptors for low-density lipoprotein, and

abnormal stromal composition [83]. However, most photosensitizers are hydrophobic and tend to aggregate easily in aqueous media, which causes a decrease in their quantum yield and problems for intravenous administration. Although many photosensitizers have been developed, few have made it to clinical trials owing to factors such as poor selectivity in terms of target tissue and healthy tissue, low extinction coefficients, absorption maxima at relatively short wavelengths, and high accumulation rates in skin [84].

Increasing the selective accumulation of the photosensitizers within the tumor tissue allows a lower effective dose of the PDT drug. One can take advantage of the intrinsic features of cancer cells, such as specific surface antigens, low-density lipoprotein receptor, and oxidation state [85]. To enhance PDT efficacy, a photosensitizer can be bound to ligands such as monoclonal antibodies or LDL, or can be delivered via carrier systems such as liposomes and micelles [86, 87]. The use of nanoparticles to improve the efficiency of PDT is a promising approach because (1) their large surface area can be modified with functional groups for additional biochemical properties, (2) they have large distribution volumes and are generally taken up efficiently by cells, (3) controlled release of drugs is possible, (4) many synthetic strategies allow transportation of hydrophobic drugs in blood, and (5) preferential accumulation in the solid tumor site is easy due to the enhanced permeability and retention effect (EPR) [88]. The latter is a phenomenon caused by the abnormal organization of the tumor neovasculature, the high porosity of the blood vessels comprising these vessels and differences in lymphatic drainage. The EPR effect facilitates both diffusion of heavy weighted PS delivery carriers into, and their retention within, tumours [89].

Nanoparticles for PDT were classified into active and passive according to the functional roles in the enhancement of PDT efficacy. Regarding active roles, they may act like catalysts to produce free radicals from dissolved oxygen, and serve as ROS modulators or light sources for activating photosensitizers. Nanoparticles such as quantum dots (QDs), up-

conversion nanoparticles, and scintillation nanoparticles can be used as light sources to activate photosensitizers due to their fluorescence emission properties [6]. Passive NPs are those acting as mere carriers of PSs. NPs for PDT were also classified by material composition into biodegradable and non-biodegradable. The formers are made of polymers that are often enzymatically hydrolyzed in a biological environment and hence release the photosensitizers. Non-biodegradable nanoparticles are used to protect the photosensitizers from the fluctuations of the environment, in which the release of the photosensitizers from the nanoparticle carriers is not necessary. Their advantages over biodegradable polymeric nanoparticles are: (1) their particle size, shape, porosity, and monodispersibility can be easily controlled during the preparation process; (2) some of them are made of inert materials which are stable to environmental fluctuations; (3) they are not subject to microbial attack; and (4) exquisite control of the pore size allows oxygen diffusion in and out of the particles but not for the drug to escape. Similarly to biodegradable nanoparticles, nondegradable nanoparticles can serve as multifunctional platforms for drug delivery [6, 88].

CHAPTER 2

TiO_2 NANOPARTICLES

2.1 Crystal Structure and Basic Photochemistry

Titanium dioxide (TiO_2) is one of the most studied photocatalyst materials by virtue of its chemical stability, low cost and nontoxicity [90]. It occurs as four major crystal structures: the stable rutile (tetragonal, a = b = 4.584 Å, c = 2.953 Å), metastable anatase (tetragonal, a = b = 3.782 Å, c = 9.502 Å), brookite (rhombohedral, a = 5.436 Å, b = 9.166 Å, c = 5.135 Å) and TiO_2 (B) (monoclinic, a = 12.16 Å, b = 3.74 Å, c = 6.51 Å). The brookite and TiO_2 (B) structures are less studied in experimental investigations. Both the rutile and anatase crystals are formed by a basic building block consisting of a titanium atom surrounded by six oxygen atoms in a more or less distorted octahedral configuration. Figure 7 depicts the unit cell structures of the rutile and anatase TiO_2. The differences in the two crystal structures are the distortion of each octahedron and the assembly pattern of the octahedral chains. In rutile, the distortion of the cubic lattice is slight so that the unit cell is stretched beyond a cubic shape. In anatase, the octahedron is significantly distorted, and thus its symmetry is lower than orthorhombic. These polymorphs determine electronic band structures, surface structure, and thus the bulk diffusion, surface transfer capability and redox potentials of photoinduced charge carriers. Among various polymorphs of TiO_2, rutile is the most stable phase for particle having a size above 35 nm, while anatase is considered to be the most thermodynamically stable for the nanoparticles with a size below 10–20 nm [91].

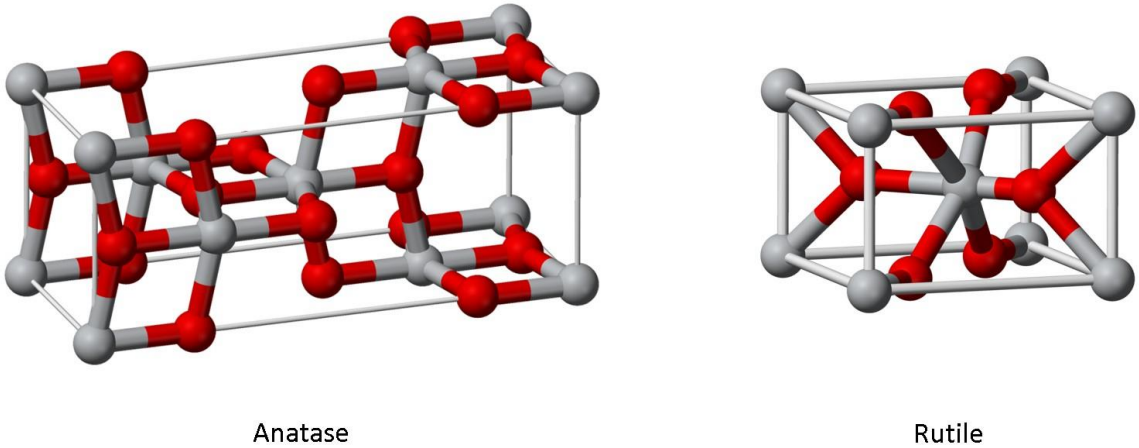

Figure 7: Bulk crystal structure of rutile (left) and anatase (right). Titanium atoms are gray, and oxygen atoms are red [91].

Photocatalysis of TiO_2 involves three processes: the excitation, bulk diffusion and surface transfer of photo-induced charge carriers. Figure 8 shows the three processes in a photocatalytic reaction [91].

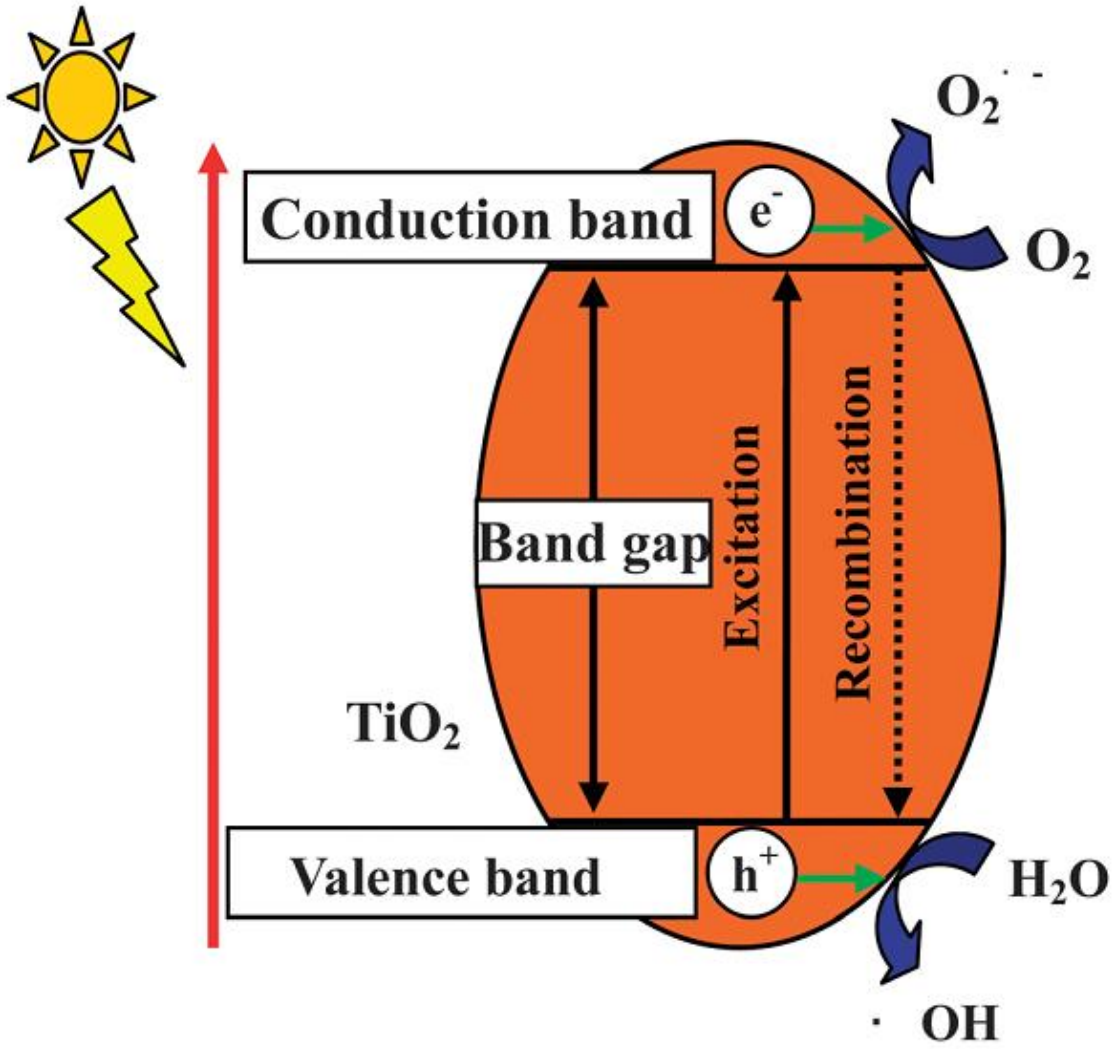

Figure 8: Schematic illustration of main processes in a photocatalytic reaction [91].

First, the semiconductor photocatalyst particles absorb a photon with energy larger than the band gap. The electrons in the valence band of the photocatalyst are excited to the conduction band. Simultaneously, the holes are left in the valence band. Secondly, the excited electrons and holes separate and migrate to the surface of the photocatalyst which is drastically affected by crystal structure, crystallinity, and by the particle size of the photocatalyst. However, recombination of photo-generated electron and hole pairs results in a decrease in the photocatalytic activity. Lastly, the electrons and holes can lead to produce surface chemical reactions. The holes can react with surface adsorbed H_2O to produce hydroxyl radicals. Meanwhile, the electrons are usually scavenged by O_2 to yield superoxide

radical anions. These species in solution can react to give other cytotoxic reactive oxygen species (ROS) such as hydrogen peroxide and peroxy radicals, which are harmful to cancer cells. The major reactions that result in the formation of ROS are shown as simplified equations (1)–(6) [91].

$$TiO_2 + h\upsilon \rightarrow h^+ + e^- \quad (1)$$

$$H_2O + h^+ \rightarrow {}^{\bullet}OH + H^+ \quad (2)$$

$$O_2 + e^- \rightarrow O_2^{\bullet -} \quad (3)$$

$$O_2^{\bullet -} + H^+ \rightarrow HO_2^{\bullet} \quad (4)$$

$$2\ HO_2^{\bullet} \rightarrow H_2O_2 + O_2 \quad (5)$$

$$H_2O_2 + O_2^{\bullet -} \rightarrow {}^{\bullet}OH + OH^- + O_2 \quad (6)$$

2.2 Photodynamic activity of TiO_2

The photo-killing activity of TiO_2 to malignant cells was first reported on a TiO_2 film electrode by A. Fujishima et al. [92]. In the system, Hela cells were cultured on the surface of TiO_2 electrode. When the electrode was anodically polarized under UV-irradiation, Hela cells were damaged from the membrane. However, cancer cells were not killed when the electrode was located 10 mm away from the cell surface, so they prepared a polarized, illuminated TiO_2 microelectrode in 1995 [93], which showed selective antitumor activity of a single cancerous T24 cell.

Considering the electrode system was not feasible and available, TiO_2 particles were applied, even nanoparticles were also prepared, which could yield an extremely large surface area and be incorporated by the living cells, resulting in higher reaction rates [91]. Under these experimental conditions, with the photo-induction of UVA, more and more researchers showed the phototoxic effect in vitro of TiO_2 nanoparticles on a series of human cancer cells, such as cervical cancer cells (HeLa) [94], bladder cancer cells (T24) [95], monocytic

leukemia cells (U937) [96] and adenocarcinoma cells (SPC-A1) [97], colon carcinoma cells (Ls-174-t) [98], breast epithelial cancer cells (MCF-7, MDA-MB-468) [99], glioma cells(U87) [100], and human hepatoma cells (Bel 7402) [91].

Importantly, the anticancer effect of TiO_2 has been also demonstrated in vivo, indicating that photo-excited TiO_2 nanoparticles may be a potential way to treat cancer in the future. R. Cai et al. [101] injected Hela cells under the skin of nude mice to cause tumors to form, when the size of the tumors grew to about 0.5 cm, they injected a solution containing fine particles of TiO_2 to the tumor. After 2 or 3 days, the skin covering the tumor was cut open to be exposed and irradiated by UVA. This treatment clearly inhibited the tumor growth. After 13 more days, the treatment was repeated and a further marked antineoplastic effect was observed. Furthermore, TiO_2 particles can significantly suppress the growth of bladder and glioma cancer cells implanted into nude mice as well, even prolong the survival time [95, 100].

2.3 Dye-Sensitized TiO_2 Nanoparticles

For practical applications, the band gap of TiO_2 (~ 3.2 eV for anatase and brookite, ~ 3.0 eV for rutile) is so large that it can be only activated under ultraviolet (UV) irradiation. UV light is also harmful to the human body, and UV only accounts for almost 5% of the sun's energy compared to visible light (45%), therefore, the shift in the optical response of TiO_2 from the UV to the visible spectral range will have a profound positive effect on the practical applications. To overcome this many modification strategies have been proposed, including doping, co-doping with two or more foreign ions, surface sensitization by organic dyes or metal complexes, and decoration with noble metal deposition [102-107].

It has been shown in 1991 by Gratzel et al. that TiO_2 nanoparticles could be sensitized with ruthenium polypyridyl complexes for the fabrication of Dye Sensitized Solar

Cells (DSSC). Significant improvement of solar cell responsiveness is possible when metallic oxides are modified by covalent attachments or adsorption of dyes [108]. TiO_2 deactivates the excited state of the ruthenium complexes via the electron transfer reaction that is on the picosecond to femto-second time scale, generating the oxidized complex form Ru (III). Consequently, in the case of aqueous media as a surrounding, the possibility of water splitting by Ru (II) polypyridyl complexes is of major interest. In fact, it is when TiO_2 is sensitized with Ru (II) polypyridyl complexes that direct water splitting is made possible with both visible light as well as near-infrared light; this is due to the fact that the difference between the potentials of the H_2/H_2O and H_2O/O_2 half-cell reactions is only 1.23 V [109]. Photo-induced electron transfer reactions in molecular donor-acceptor dyads and in sensitizer-semiconductor dyads often result in high quantum yield for transient photochemical charge separation. Hydrogen or oxygen can be made in good quantum yield if these systems are coupled to sacrificial electron donors or acceptors, Figure 9 [110].

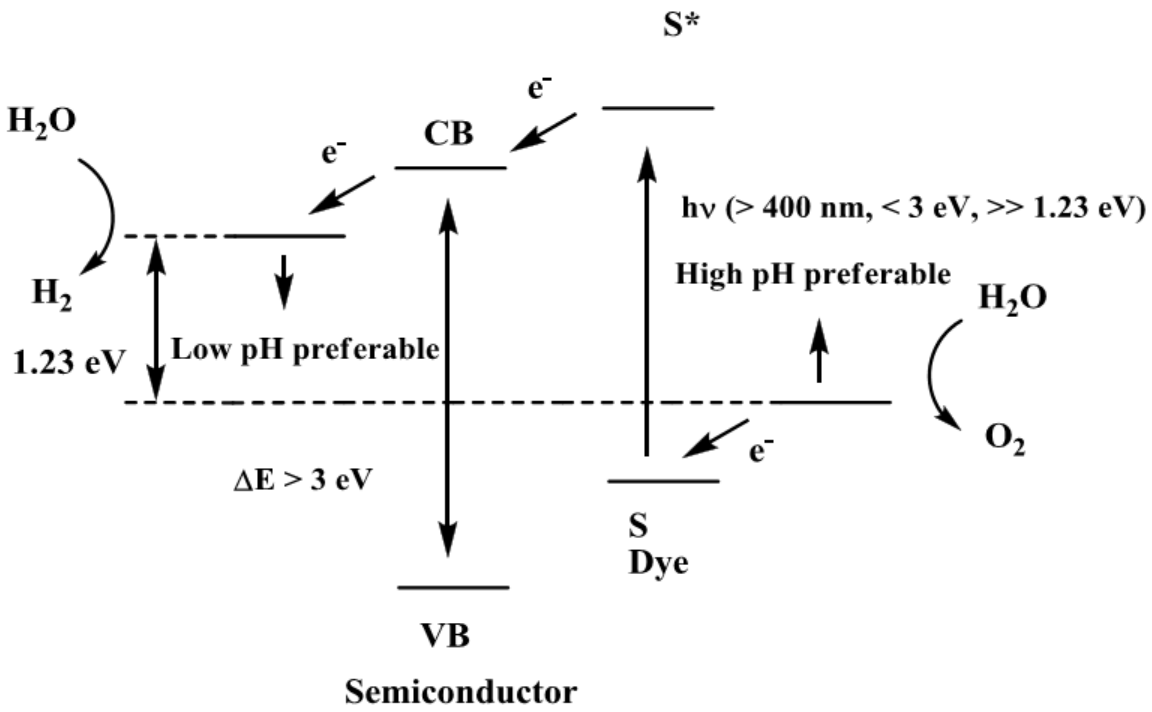

Figure 9: Scheme illustrating forward electron transfer in sensitized TiO2 in aqueous systems [109].

Generally, water splitting by visible light requires two electrons for hydrogen formation and four electrons for oxygen formation, and this corresponds to the most favorable thermodynamic conditions for the reaction to take place. It is a multi-electron process that requires 1.23 eV per electron transferred [111]. The energies required for the reactions of the formation of radical intermediates are considerably higher when compared with those of multi-electron reactions that require -0.414 V and +0.816 V at pH = 7 versus NHE, for the H_2 and O_2 evolving reactions, respectively. These reactions with their required corresponding energies are summarized in the following equations:

$$H^+ + e^- \longrightarrow H^\bullet \qquad E^o = -2.61\ V$$

$$2\ OH^\bullet + 2H^+ + 2\ e^- \longrightarrow 2\ H_2O \qquad E^o = 2.31\ V$$

$$2H^+ + 2e^- \longrightarrow H_2 \qquad E^o = -0.41\ V$$

$$O_2 + 4H^+ + 4\ e^- \longrightarrow 2\ H_2O \qquad E^o = 0.82\ V$$

$$H_2O_2 + 2H^+ + 2\ e^- \longrightarrow 2\ H_2O \qquad E^o = 1.35\ V$$

Therefore, successive one-electron oxidations of water molecule yield $O_2^{-\cdot}$, H_2O_2, $HO^\cdot$ and O_2. A potential diagram that includes the redox potentials at pH = 7 for one- two- and four-electron couples that involve these states is shown in Figure 10 [112].

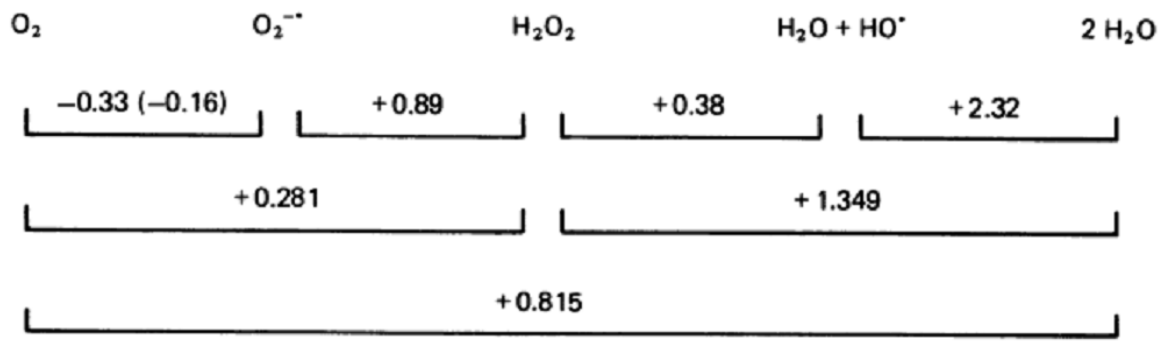

Figure 10: Potential diagram for water at pH = 7 [112].

2.4 Photodynamic Activity of Dye Sensitized-TiO_2 Nanoparticles

Janczyk et al. investigated the photodynamic activity of platinum(IV) chloride sensitized TiO_2 NPs. In vitro experiments with the mouse melanoma cells (S-91) and murine macrophage cell line (RAW 264.7) have demonstrated phototoxicity of the material through efficiently generated various reactive oxygen species (•OH, $O_2^{\bullet-}$, H_2O_2, $^1O_2$) and also reactive chlorine species induced by visible light irradiation (λ > 455 nm) [113, 114]. Similarly, Lei et al. extended the absorption spectrum of TiO_2 NPs by attaching ascorbic acid (AA) molecules to their surfaces. Upon visible light irradiation (>550 nm), TiO_2-AA hybrids were able to transform supercoiled DNA into linear form. The group found that •OH, $O_2^{\bullet-}$, and $^1O_2$ were the reactive agents contributing to the DNA cleavage. The drawback of this method is that AA is irreversibly oxidized to dehydroascorbic acid and would not regenerate inside a cell [115]. Recently, there have been a few reports on the sensitization of TiO_2 with known organic and metallorganic photosensitizers, clinically approved or presently investigated for PDT. Such combination can potentially yield a synergistic effect of the assembly in tumor therapy. For example, Tokuoka *et al.* attached an FDA approved porphyrin photosensitizer, chlorin e6, to TiO_2 NPs. Irradiation of polychromatic light (550–750 nm), that excites chlorin e6, significantly damaged the EL-4 cells and a higher cell-killing effect was found for the dye-TiO_2 particles than for the system using chlorin e6 alone [116]. Lopez *et al.* incorporated an efficient photosensitizer, Zinc phthalocyanine (ZnPc) molecules, into the porous network of TiO_2 using the sol-gel method. However, the photodynamic effect of the composite TiO_2-ZnPc on tumor and non-malignant mammalian cells was less potent than that of pure ZnPc alone. The authors attributed this result to the fact that the composite material was less internalized by the cells than the pure dye was [117].

CHAPTER 3

DESIGN OF RUTHENIUM POLYPYRIDYL-SENSITIZED TiO_2 HYBRID NANOPARTICLES

Based on our group's background in the research area of dye-sensitized solar cells (DSSCs), we set to develop ruthenium polypyridyl dyed titania-based hybrid NPs that follow Type I PDT mechanism exclusively. To that end, core-shell-shell magnetite-silica-titania nanoparticles Fe_3O_4@SiO_2@TiO_2 (C-NPs) were synthesized by successive sol-gel methods, Scheme 1. The super-paramagnetic magnetite cores can be used as contrast agents for MRI as previously mentioned, and with the application of an external magnetic field at the tumor site, their accumulation and retention in the target tissue can be greatly enhanced. Next, a ruthenium dye, $[(4,4'\text{-dcbpy})_2\text{Ru(dm-bpy)}].2Cl$ (where dc = dicarboxy, dm = dimethyl, and bpy = 2,2′-bipyridine), was anchored to the nanoparticles forming the hybrid photosensitizer Fe_3O_4@SiO_2@TiO_2@Dye (D-NPs). The role of titania, is to accept the electron injected from the photo-excited dye into its conduction band (similar to how DSSCs work). Theoretically, both the holes in the oxidized dye and accumulated electrons in TiO_2 can oxidize and reduce, respectively, surrounding species (especially oxygen and water) to form cytotoxic free-radicals (PDT Type I). The silica buffer layer between magnetite and titania is necessary since SiO_2 acts as an insulating layer preventing electron-hole recombination at the magnetite center, thus increasing the lifetime of the photo-generated holes (at the dye end) and electrons (at the titania end), and hence their photo-reactivity [118].

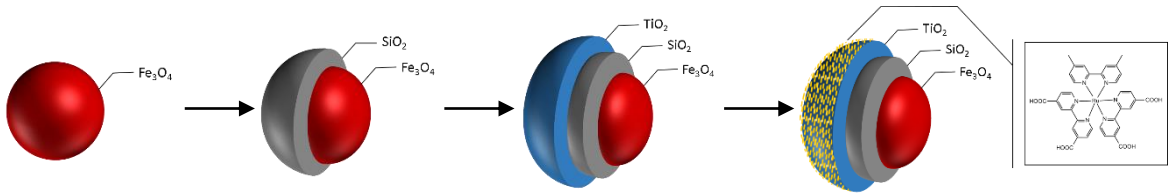

A-NPs B-NPs C-NPs D-NPs

Scheme 1: schematic representation of A, B, C and D nanoparticles.

The Fe_3O_4@SiO_2@TiO_2 nanocomposites are sensitized with a polypyridyl ruthenium complex through the latter's CO_2H groups, resulting in a coupling interaction between the photosensitizer energy levels and the energy bands of the TiO_2 semiconductor and their photosensitizing powers are measured by the degree of ROS generated upon light irradiation. Upon photoexcitation, an efficient electron injection from the dye into the conduction band of the semiconductor takes place as an ultrafast process on the femtosecond scale. Consequently, TiO_2 will deactivate the excited state of the ruthenium complexes via the electron transfer generating the oxidized complex form Ru (III). The strong oxidizing power of Ru (III) complexes (E_{ox} ~ 1.5 eV versus NHE) leads to direct and indirect oxidation of species within the cells such as peptides and DNA bases. However, the lifetime of the oxidized metal center should be long enough for redox reactions to take place, and this is the case of Ru (III) that lives between 0.1 to 20 ms when anchored to TiO_2 [119]. As a result, highly destructive radical species could be generated causing oxidative damage to cells and subsequent cell death. Also cell damage could take place reductively by electron transfer from the conduction band of the TiO_2 semiconductor to the accepting species in the cell.

Fe_3O_4@SiO_2@TiO_2 NPs synthesis has been reported in the literature using different methods, but their applications, whether bare or with a photosensitizer's assistance, have been focused on their photocatalytic activity for water purification mainly [118, 120-130]. To our knowledge, the use of ruthenium polypyridyl complexes-sensitized metal oxides in PDT has never been reported. Recently, Truillet, C. *et al.* synthesized gadolinium based nanoparticles with a Ru(II) polypyridyl complex covalently grafted on the inorganic magnetic matrix in order to obtain MRI/PDT multifunctional platforms [131]. Although these hybrid nanocomposites demonstrated *in vitro* cytotoxicity, the ruthenium-based complex didn't sensitize the metal oxide; the latter was only a MRI contrast agent and a mere support for the

dye generating the singlet oxygen species in the medium. In this thesis work, we demonstrate the effective cytotoxic properties of this novel composition of NPs in an *in vitro* model of human lung cancer cell line (A549 cells).

CHAPTER 4

EXPERIMENTAL

4.1 Instruments and Equipment

X-Ray diffraction measurements were performed using Bruker D8 Discover. Fourier transform infrared (FT-IR) spectra were collected on Nicolet 4700, Thermo Electron Corporation. The surface areas of the different samples were calculated according to Brunauer-Emmet-Teller (BET) model from nitrogen adsorption isotherms carried out on Nova 2200e Surface Area and Pore Size Analyzer, Quantachrome Instruments. Throughout the work, NP samples were concentrated using Amicon® pressure-based stirred cells diafiltration set-up, Figure 11. Energy-dispersive X-ray spectroscopy (EDX) spectra and scanning electron microscopy (SEM) images of the nanoparticles were obtained using Tescan Mira 3 MLU, and X-Max Silicon drift detector with 20 mm^2 detector size, Oxford Instruments. The hydrodynamic radii of the NPs were measured using 90Plus Particle Size Analyzer, Brookhaven Instruments Corporation. Total reactive oxygen species (ROS) and singlet oxygen generations were assessed by measuring the emission of a fluorescent probe using Fluorolog FL-1057 from Horiba Jobin Yvon, and the UV-Vis spectra of another probe using Jasco V-570, respectively. Images of excitation and viability of A549 cells were captured with two channels 488nm (Calcein) and 561nm (PI) using LSM710 confocal microscope (Zeiss, Germany). In case of ROS production, images were immediately captured after excitation at 520nm (DHE) and 488nm (DCF).

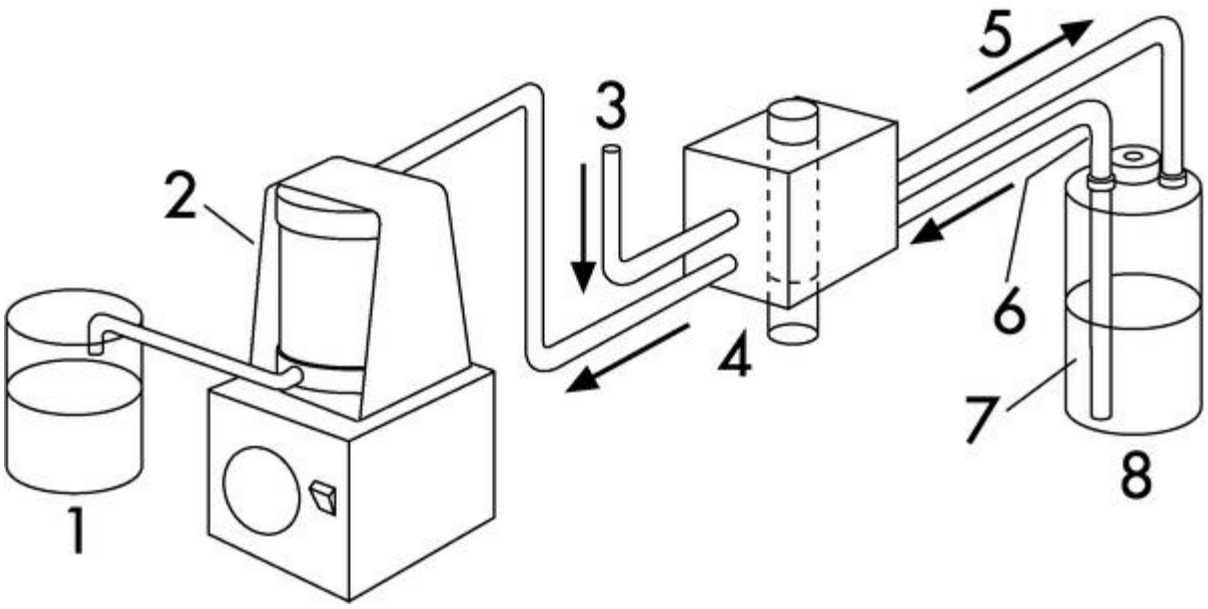

Figure 11: Diafiltration set-up and operation with Amicon selector valve, stirred cell and accessory reservoir. 1 - Ultrafiltrate, 2 - Ultrafiltration equipment, 3 - Pressure supply, 4 - Selector valve, 5 - Inlet, 6 - Outlet, 7 - Feed liquid, 8 - Reservoir

4.2 Materials

Iron (II) chloride tetrahydrate ($FeCl_2.4H_2O$) (99%), Iron (III) chloride hexahydrate ($FeCl_3.6H_2O$) (97%), Propidium iodide (PI), and fluorescein isothiocyanate were purchased from Sigma-Aldrich. Tetraethyl orthosilicate (TEOS) ($C_8H_{20}O_4Si$) (99%), Poly (acrylic acid, sodium salt) $–(C_3H_3NaO_2)-_n$ (Mw ≈ 2,100), 9,10-dimethylanthracene (DMA), and 3-Hydroxytyramine hydrobromide were obtained from Aldrich. Titanium (IV) isopropoxide ($C_{12}H_{28}O_4Ti$) (98%) was purchased from Acros Organics and Degussa P25 titania from Sigma-Aldrich. Sodium phosphate monobasic ($NaHPO_4.H_2O$) from Fisher Scientific Company and sodium phosphate, dibasic, anhydrous (Na_2PO_4) from Solar Laboratories, Inc. were used to make phosphate buffer solutions. 2,7-Dichlorodihydrofluorescein diacetate (DCFH-DA) was purchased from Cayman Chemical Company. Dihydroethidium (DHE) and Calcein-AM were purchased from life technologies. Glass Bottom Culture Dishes (Confocal dishes) were purchased from Matek®(USA), glass bottom 8 well chambers from BD falcon-USA. For cell culture, DMEM AQ culture media, Penicillin G, Streptomycin, Fetal Bovine Serum and Sodium Pyruvate were ordered from Sigma-Aldrich. Solvents, and other

chemicals, were of analytical grade and used without further purification. Distilled and deionized water was used throughout the work.

Synthesis of Polyacrylic-Acid-Capped Iron Oxide Nanoparticles (PAA-Fe3O4), (A-NPs):

Stable Fe_3O_4 ferrofluid was synthesized using the method of coprecipitation of Fe(II) and Fe(III) salts in the presence of PAA oligomer as a surfactant as reported elsewhere [132, 133] with modifications. Typically, 5.57 g (21.24 mmol) of $FeCl_3.6H_2O$ and 2.01 g (10.21 mmol) of $FeCl_2.4H_2O$ were dissolved in 100 ml of water inside a 500 ml 3-necked round bottom flask (RBF). Separately, 1.74 g of PAA were dissolved in 50 ml of water then transferred into the RBF. The mixture was probe sonicated for 15 min, followed by purging with nitrogen gas for 20 minutes while heating it up to 60°C. Next, under vigorous mechanical stirring, excess NH_4OH (10 ml, 28% by weight) were quickly added to the reactor using a syringe. Upon addition of the ammonium solution, the color of the mixture turned from orange to black immediately. The temperature was raised to 90°C over 15 min and stirring was continued for another 45 min. The resultant solution was left to cool down to room temperature and then filtered under pressure against water until it became neutral (the pH of the filtrate was periodically checked using a litmus paper). The final concentration was found to be ≈ 32 mg/ml of water.

Coating of Nanoparticles with Silica to get Fe3O4@SiO2, (B-NPs):

Following the Stober method [134], with modification, the coating of magnetite nanoparticles with silica was carried out in a basic ethanol/water mixture at 25°C. In a 5-liter 3-necked RBF, 20 ml of PAA-Fe_3O_4 solution were diluted in a 640 ml of water and 1920 ml of ethanol, then probe sonicated for 30 min. Next, excess NH_4OH (48 ml, 28% by weight) was added to the solution before it was deaerated with nitrogen for 30 min. Then, under vigorous mechanical stirring, 4.8 g (28.54 mmol) of TEOS diluted in 320 ml of ethanol were added drop-wise from a separatory funnel as slow as possible; and stirring was continued for

12 h. The resultant solution was probe sonicated for 30 min and then pressure filtered against ethanol to a final concentration of ≈ 12 mg/ml of ethanol.

Coating of Nanoparticles with Titania to get Fe3O4@SiO2@TiO2, (C-NPs):

Coating of nanoparticles with titania was carried out using the sol-gel method as reported elsewhere with modifications [118]. Typically, 71 ml of silica-coated NPs were diluted into 3270 ml of ethanol then probe sonicated in a 5-liter RBF for 30 min. separately, under rapid magnetic stirring at 0°C, 8.54 ml (29.12 mmol) of titanium isopropoxide were added to 430 ml of isoproponal. Stirring of the isopropoxide solution was continued for 5 min. Next, under vigorous mechanical stirring at 50°C, the titanium sol was added drop-wise to the reactor over 3 hours. The solution was left to age at 50°C for 4 hours, before adding 30 ml of water. The reaction was left stirring at 60°C for an extra 30 min. After 24 h, it was probe sonicated for 30 min, and then pressure filtered against water making sure no traces of ethanol are left. The final volume of the solution was adjusted to 80 ml. The solution was hydrothermally treated inside an acid digestion bomb at 200°C for 24 h. The final concentration of this solution was measured to be 19.6 mg of NPs per ml of water.

Anchoring of Ruthenium dye on titania-coated NPs (Fe3O4@SiO2@TiO2@Dye), (D-NPs):

The inorganic dye used was $(dc\text{-}bpy)_2Ru(dm\text{-}bpy).2PF_6$ (Dye) where dc-bpy is 4,4′-dicarboxy-2,2′-bipyridine, dm-bpy is 4,4′-dimethyl-2,2′-bipyridine. This dye was available from previous work [119]. To anchor it to titania-coated NPs, a solution of the latter was pressure filtered against ethanol until it became water free. Next, excess dye in ethanol was added to the filtered C-NPs solution, bath sonicated for 30 min, and then left in the dark overnight. After 24 h, the solution was washed multiple times by centrifugation until the supernatant solution obtained after centrifugation was colorless. The concentration of NPs in this solution was found to be 9.5 mg/ml of ethanol.

Total ROS generation in solution measurements:

To measure ROS generated by D-NPs in solution, a PBS, 0.1 M, was prepared, and a solution of DCFH, 3.5 mM, was reconstituted by dissolving DCFH-DA in 10 mM NaOH. Next, 3 ml of PBS and 10 µl of DCFH were transferred into a quartz cuvette. Finally, 0.5 mg of various NP solutions (A-NPs, B-NPs, C-NPs, D-NPs, Deguassa P25 TiO_2 NPs) was added. The solution inside the cuvette was then exposed to either green (532 nm, 5 mW) or white light while (with a UV filter up to 350 nm) bubbling it with air to ensure oxygen saturation, and the emission spectrum (λ_{ex} = 500 nm, λ_{em} = 520 nm) was recorded at different intervals with light being on for 5 min and off for another 5, Figure 12.

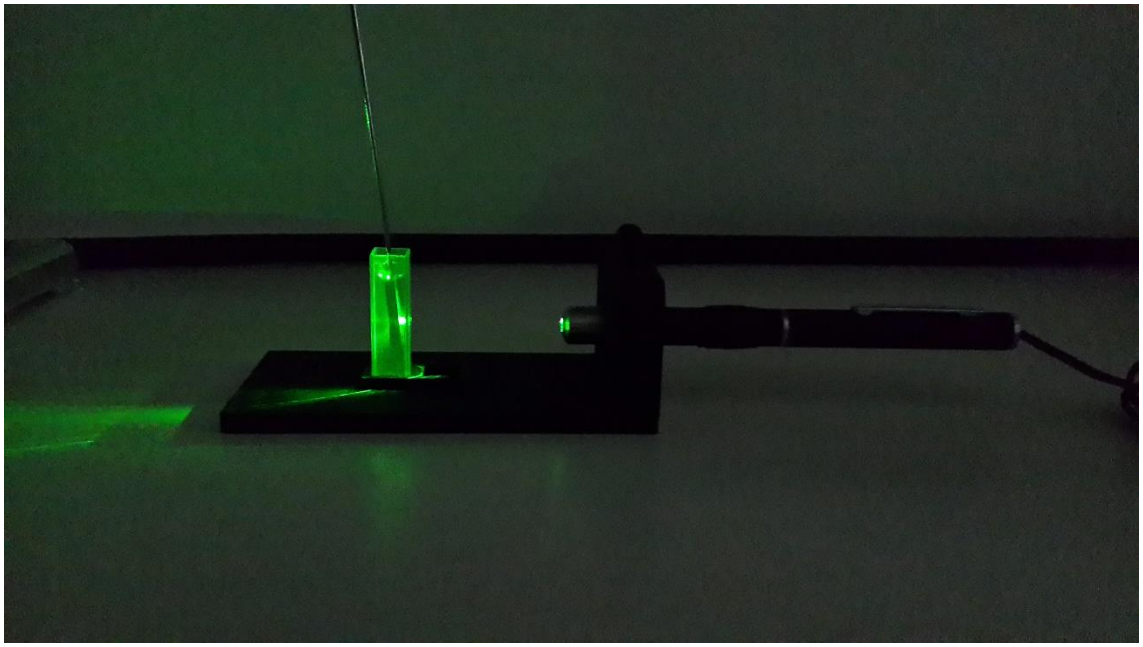

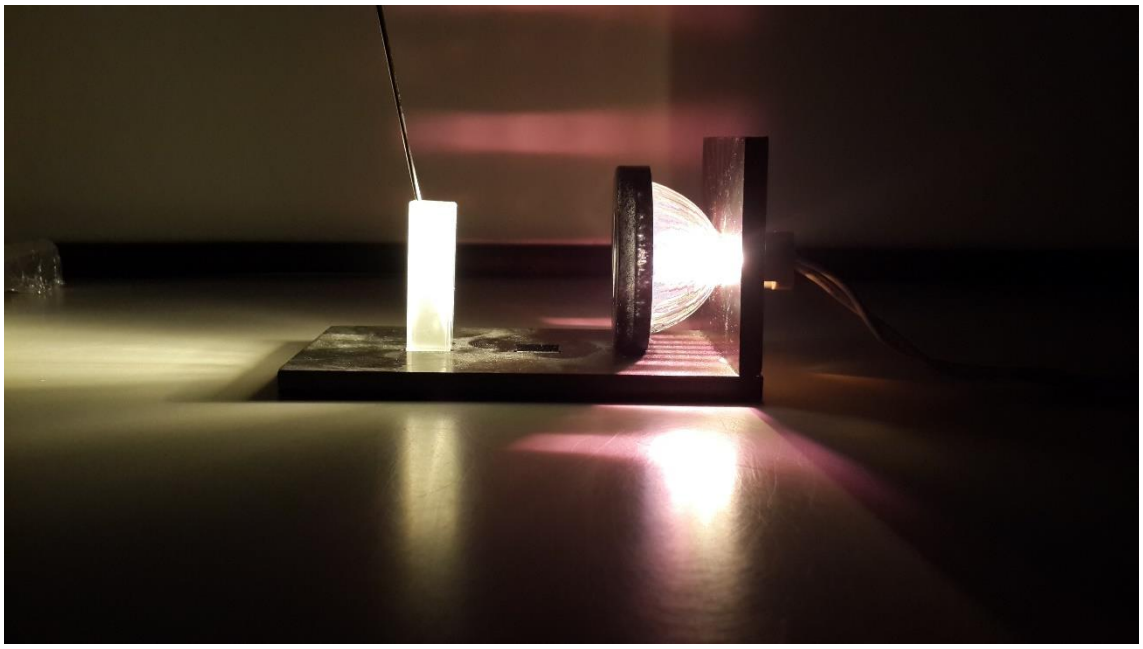

Figure 12: The setup of the total ROS generation in solution. Excitation with green light (top) and white light (bottom) were carried out.

Singlet oxygen generation in solution measurements:

Singlet oxygen generation was measured using DMA as a probe. 2 solutions were prepared: the first contains 7.5 x 10^{-5} M DMA and 1.5 x 10^{-5} M of Dye, and another one having the same concentration of DMA plus 0.408 mg of D-NPs. UV-Vis and emission spectra (λ_{ex} = 397 nm, λ_{em} = 410-600 nm) were recorded at t = 0 (immediately upon adding Dye or D-NPs) and after 80 min of excitation using the same green light used before, Figure 12. Again, both solutions were bubbled with air throughout the experiment.

Measuring the quantity of Dye anchored to the NPs in D-NPs:

Dye was desorbed from D-NPs upon addition of aqueous NaOH. The resultant solution was centrifuged and the UV-Vis spectrum of the supernatant was measured. The concentration of the dye in the solution and hence its amount anchored on the NPs were calculated ($\mathcal{E}_{475\ nm}$ ≈ 17000 l.mol^{-1}cm^{-1}). Concentration of Dye was calculated to be 50 mmol/g of NPs.

Cell culture:

A549 cells, a human lung adenocarcinoma epithelial cell line, were grown in DMEM AQ culture media supplemented with Penicillin G 100 U/ml and Streptomycin 100 µg/ml, 10% Fetal Bovine Serum (FBS) and Sodium Pyruvate. Cells were cultured in a 37 °C incubator with 5% CO_2 atmosphere.

Cellular uptake of nanoparticles:

We assessed the uptake of NPs into A549 cells using two independent methods: flow cytometry and microscopy. In flow cytometry experiments, we quantified the uptake of fluorescein isothiocyanate (FITC) labeled C-NPs (FITC-C-NPs) by cells. The latter were prepared by adding excess dopamine to C-NPs and leaving them over night. The next day, the NPs were captured, using a strong magnet, and washed multiple times with water to remove the remaining free dopamine. The FT-IR spectrum of the resulting NPs confirmed the presence of dopamine on the nanocomposites. Next, excess FITC in ethanol was added to the resulting NPs solution, and was left overnight. The next day, the remaining free FITC was removed by washing using ethanol multiple times, then water, to obtain FITC-C-NPs .Cells were seeded in 6-well plates (10^4 cells/cm^2) until reaching 50% confluence after which FITC-C-NPs were added. At different time points, cells were washed, trypsinized, and collected by centrifugation at 100g and re-suspended in 4% formaldehyde with gently vortex to avoid cell clumping. Cell suspensions were analyzed by flow cytometry where fluorescence intensity was plotted for each sample.

Nanoparticles internalization was also assessed by fluorescence microscopy. A549 cells, seeded in confocal dishes, were loaded with FITC-C-NPs overnight. Before imaging, calcein-blue AM (Invitrogen), a blue fluorescent cell marker dye, was added. After thorough washing of the un-internalized dye, we acquired 3D images of the cells using a laser scanning confocal fluorescent microscope.

Excitation and Viability Measurements of A549 Cells:

A549 cells were seeded in glass bottom 8 well chambers (5000 cells/well). After 24 h, cells were treated with D-NPs or left untreated. For treatment, D-NPs were suspended in 95% ethanol and adjusted to 1 mg/ml. A solution of 1% v/v was added to 1 ml of media resulting in a concentration of 10 μg/ml. After 24 h of incubation, cells were washed to remove unbound D-NPs. One 8 well chamber was covered with aluminum foil and one was kept uncovered. The 8-well chambers were then placed on the surface of a projector light, and excited for 15 minutes with a halogen lamp. Light output was measured to be 100 $mW.s^{-1}$. Following excitation, the 8-well chambers were imaged and then placed in a humidified CO_2 incubator. After 16 h of incubation, calcein-AM was added to each well and images were obtained. Calcein-AM is a permeable dye that enters the cells where endogenous esterases cleave the AM group rendering the now fluorescent calcein impermeable. Living cells retain the dye within the cytoplasm while dead cells lose the dye. Fluorescence microscopy and bright field imaging were performed and living cells were counted in an automated way using Cell Profiler software while dead cells were counted manually by looking for cells that had lost the calcein fluorescence.

Measurement of Intracellular ROS:

Intracellular ROS generation was assessed in A549 D-NPs-treated cells by an ROS sensitive dye, Dihydroethidium (DHE). Dihydroethidium was used according to the manufacturer's protocol. Cells were cultured in confocal dishes, treated with D-NPs overnight, washed with PBS and incubated with 3 μM DHE at 37° C for 15 min. Cells were then excited for 5 min and live imaged at 520 nm.

CHAPTER 5

RESULTS AND DISCUSSION

Core-shell-shell magnetite-silica-titania nanoparticles (C-NPs), Scheme 1, were synthesized by successive sol-gel methods. The magnetite cores (A-NPs) were electrostatically stabilized and dispersed by the addition of polyacrylic acid. Infrared, energy-dispersive X-ray and X-Ray diffraction measurements of the multilayered NPs confirmed the presence of the surfactant polymer and the three oxides. Figure 13 shows the FT-IR spectra of PAA alone, and those of the NPs at different stages of their synthesis. The strong band at ca. 1710 cm^{-1} in PAA spectrum is attributed to the carbonyl group stretching mode [135]. The appearance of the latter in the spectrum of A-NPs with a lower intensity is indicative of the presence of PAA in the magnetite NPs [136]. The spectrum of A-NPs also exhibits the characteristic absorption band of Fe-O stretching vibration at 582 cm^{-1} as previously reported [132]. The spectrum of B-NPs shows the symmetric and asymmetric vibrations of Si-O-Si at around 800 and 1080 cm^{-1}, respectively [125]. The broad band in the spectrum of C-NPs between 500 and 800 cm^{-1} is that of Ti-O-Ti vibration modes [125].

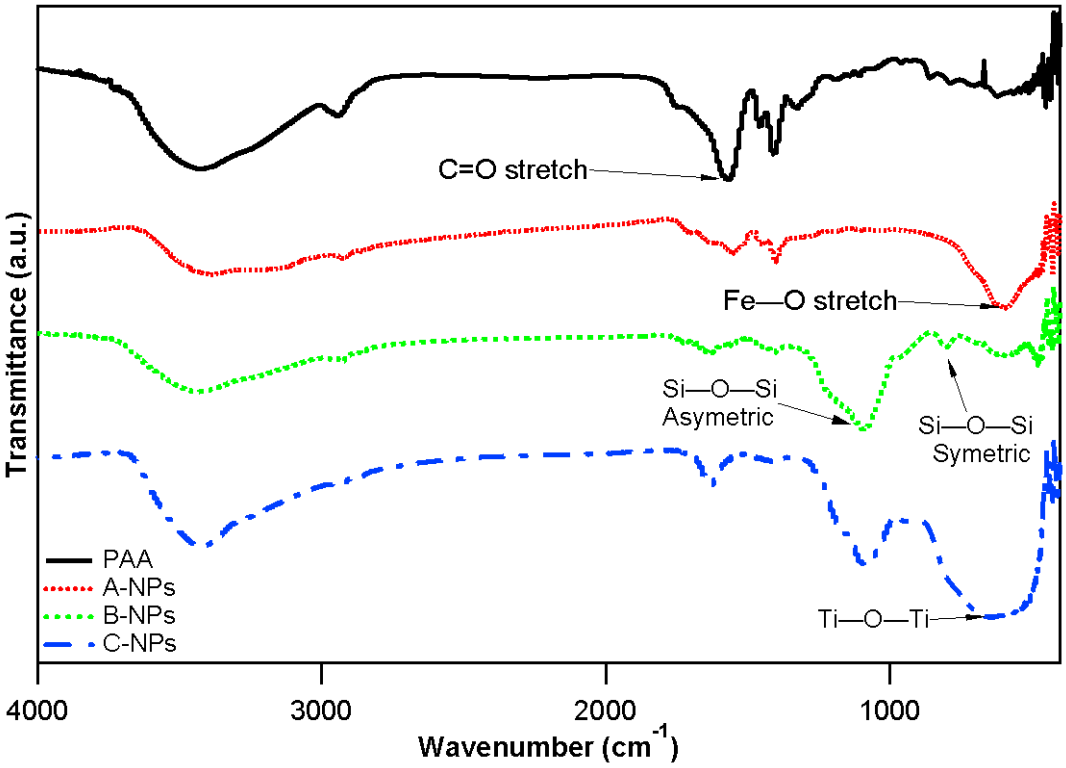

Figure 13: FT-IR spectra of PAA (solid-black), A-NPs (dotted-red), B-NPs (dashed-green), and C-NPs (dashed-dotted-blue).

The X-ray diffraction patterns of the different NPs are presented in Figure 14. The XRD pattern of A-NPs was in agreement with the JCPDS card No. 19-0629, presenting the characteristic peaks at 2θ: 30.4° (220), 35.7° (311), 43.4° (400), 53.8° (422), 57.4° (511) and 63.0° (440) of cubic spinel structure of magnetite [122]. Coating the Fe_3O_4 cores with SiO_2 didn't change the structure of the former as can be seen in the diffractogram of the B-NPs. The XRD pattern of the latter show the attenuation of the Fe_3O_4 peaks, and a new broad peak between 20° and 28° which is indicative of the amorphous nature of the SiO_2 layer [122]. The diffractogram of the C-NPs comprises peaks for TiO_2 layer along with those of the magnetic core. The peaks at 25.4° (101) and 48.1° (200) are characteristic of the anatase polymorph of TiO_2 (JCPDS card No. 21-1272) [137].

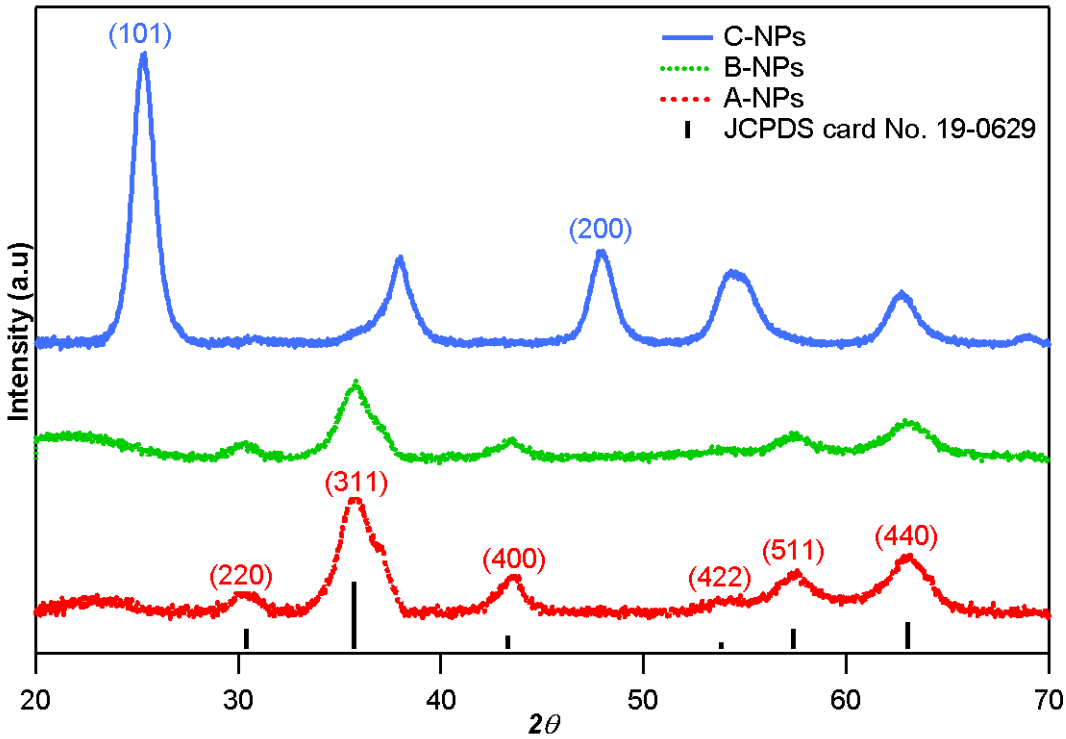

Figure 14: XRD diffractogram of A-NPs (dashed-red), B-NPs (dotted-green), and C-NPs (solid-blue) in addition to JCPDS card No. 19-0629 of Fe3O4.

The energy dispersive x-ray spectroscopy analysis of the different NPs showed the presence of the 5 expected elements: C, O, Fe, Si, and Ti. The relative percentage of iron to silicon was consistent at 2:3 in both the silica coated and the titania coated samples, Table 2.

Table 2: Percentage of oxygen, iron, silicon and titanium in each sample as obtained from EDX measurements

Sample	Oxygen	Iron	Silicon	Titanium
B-NPs	-	39.37	60.63	-
C-NPs	-	12.10	17.55	70.35

The morphology of the various nanocomposites was characterized by SEM, Figure 15. The NPs had a nearly spherical shape at the different stages of their synthesis. Figure 15 also shows the particle size distributions obtained from SEM images of the different NPs. The mean equivalent diameters of the nanocomposites are summarized in Table 3.

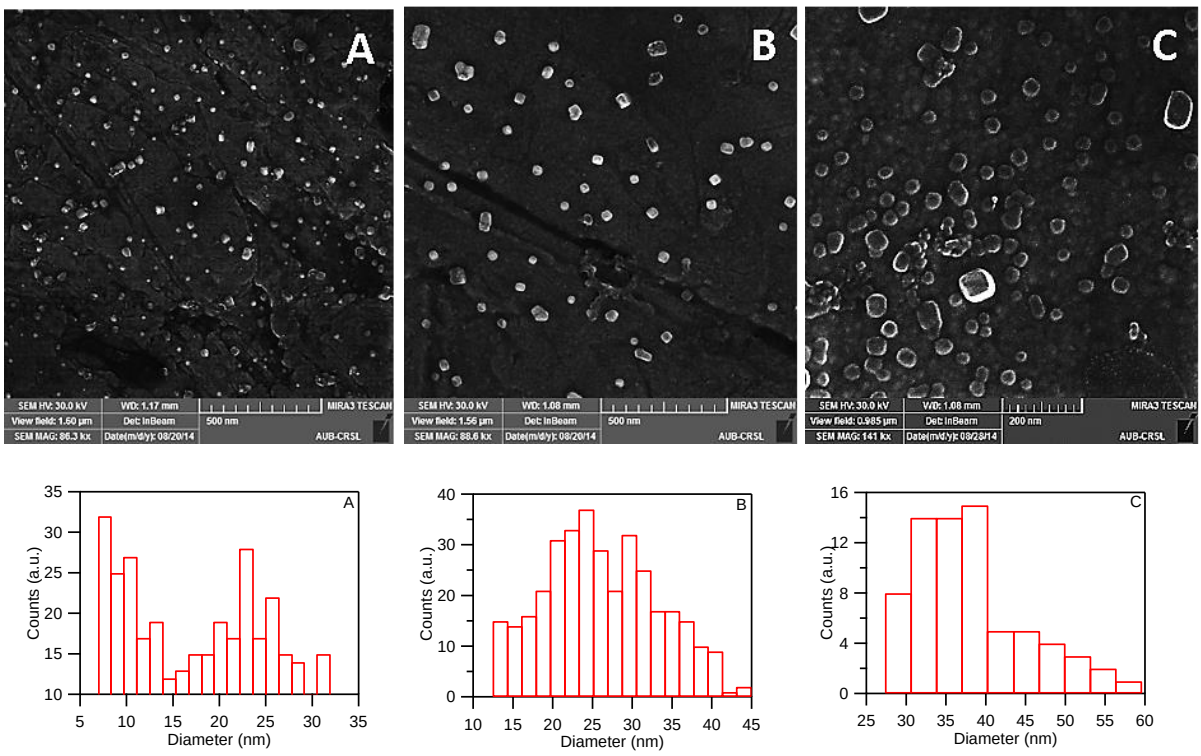

Figure 15: SEM images of the different nanoparticles A-NPs, B-NPs and C-NPs (above) and The particle size distributions obtained for each from SEM (below).

Table 3: Mean diameters of the different NPs obtained by SEM and DLS.

Sample	SEM mean equivalent diameter (nm)	DLS number-weighted mean diameter (nm)	DLS intensity-weighted hydrodynamic diameter (nm)
A-NPs	17	17	62
B-NPs	27	26	90
C-NPs	40	33	99

The hydrodynamic diameter of the different nanocomposites was measured using DLS, Figure 16 and table 3. The intensity-weighed mean diameter grew from 62 nm for A-NPs to 90 nm for B-NPs, and to 99 nm for C-NPs, which is within the optimum size range for cellular uptake [138]. The intensity-weighed values can also be converted mathematically to number-weighed ones which can be directly compared to the mean equivalent diameters obtained by the SEM. The values obtained for the different NPs by the two instruments were comparable, Table 3.

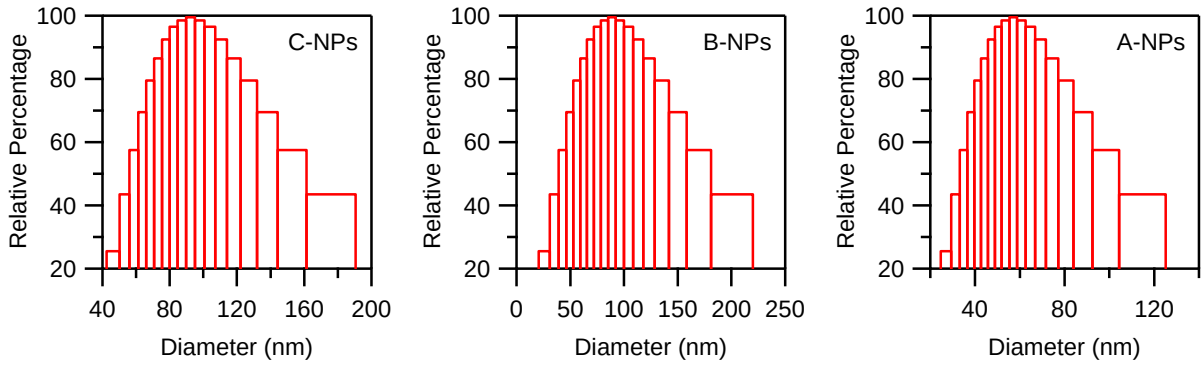

Figure 16: DLS intensity-weighed hydrodynamic diameter distribution of A-NPs, B-NPs, and C-NPs.

Brunauer-Emmett-Teller (BET) surface areas for the different nanocomposites are summarized in Table 4. The surface area increased with the addition of each coating layer but then decreased following the hydrothermal treatment. This suggests that the increased crystallinity of TiO_2 achieved by the treatment was accompanied by a deterioration of its porous structure.

Table 4: BET surface area of the different NPs.

Sample	BET Surface Area (m^2/g)
A-NPs	95
B-NPs	145
C-NPs (before hydrothermal treatment)	233
C-NPs (Hydrothermally treated)	126

The total ROS generation in solution was measured using Dichloro-dihydro-fluorescein (DCFH) as a probe, Scheme 2. The latter is a non-fluorescent molecule, however, in the presence of ROS in solution, it's readily oxidized to DCF which is highly fluorescent [139].

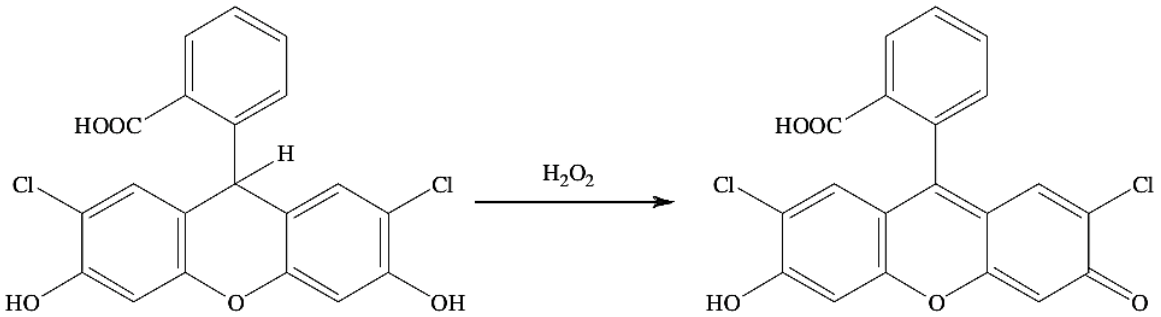

Scheme 2: reaction of the conversion of DCFH to DCF in the presence of free radicals [139].

The emission fluorescence intensity at 520 nm of several samples (Blank, A-NPs, B-NPs, C-NPs, D-NPs, Dye, and Deguassa P25 TiO_2 NPs) were measured at successive excitation with green light, or white light, Figure 17 top and bottom, respectively. The results of A-NPs and B-NPs were comparable to the blank/control trials. Degussa P25 TiO_2 NPs generated slightly higher intensities. ROS generated by the Dye and C-NPs showed similar effectiveness in oxidizing DCFH, however, neither of which achieved what D-NPs were able to. After the first excitation which lasted for 5 min, the NPs were left in the dark for 5 min and then were excited again for another 5 min. the further increase in DCF fluorescence intensity indicates that more ROS has been generated following every excitation (a similar trend was observed after 2 more excitations, but data are not shown). After 2 excitations only, D-NPs generated more than 5 times with green light and around 4 times with white light what any of the other samples were able to. The fact that the quantity of ROS generated can be controlled by the frequency of excitations means that photo-treatments can be repeated until the desired therapeutic effect is achieved.

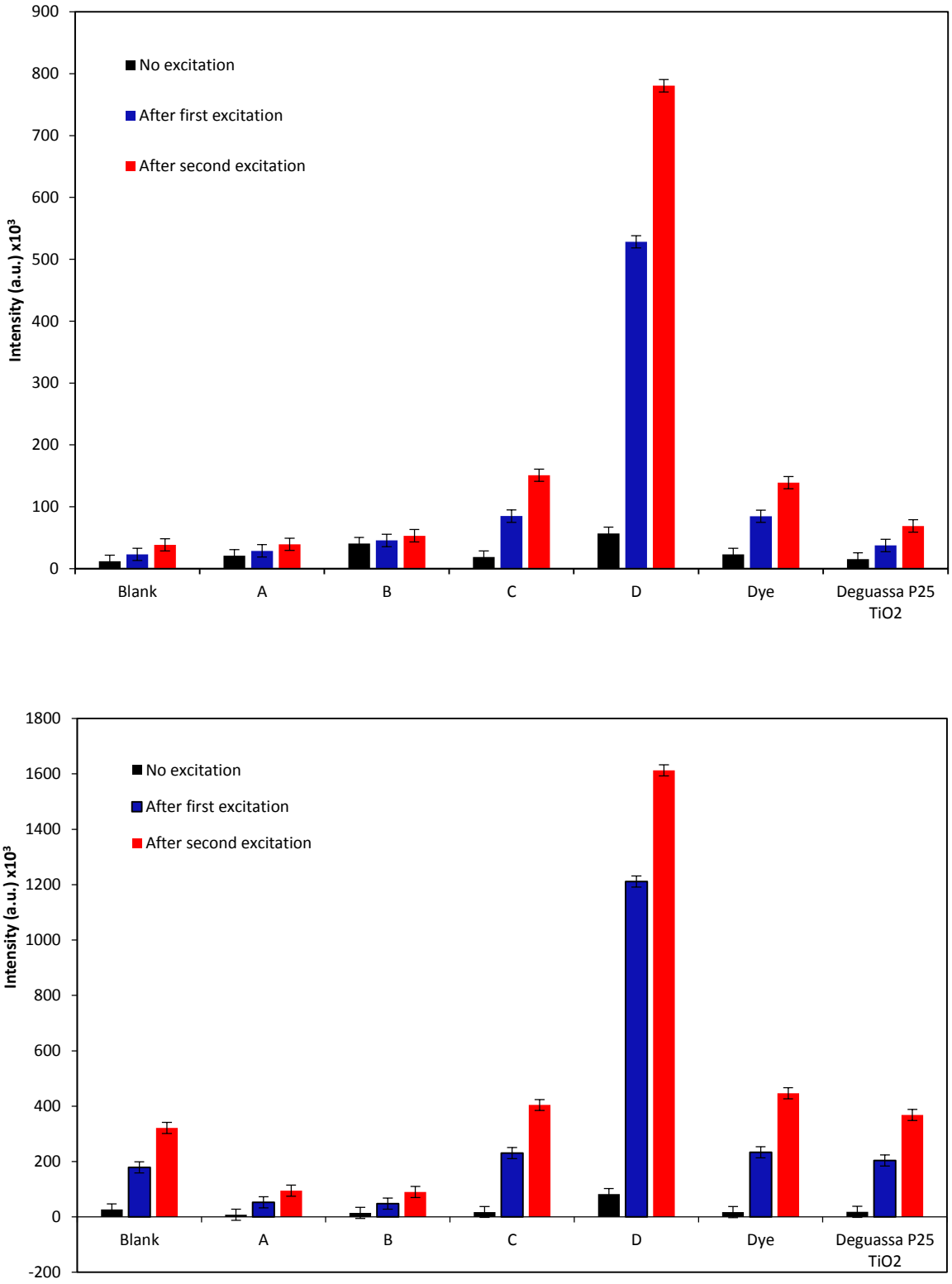

Figure 17: Fluorescence intensities of DCF at 520 nm after successive 5 min intervals light excitation (top: green light, bottom: white light) of a blank control, A-NPs, B-NPs, C-NPs, D-NPs, Dye, and Deguassa P25 TiO2 NPs. Excitation intervals were separated by a 5 min in-dark interval.

In the second set of experiments, we chose a singlet-oxygen-specific molecular probe 9,10-dimethylanthracene (DMA), to measure if any $^1O_2$ is generated by D-NPs. DMA is a fluorescent compound ($\lambda_{excitation} = 375\ nm, \lambda_{emission} = 436\ nm$) that reacts selectively with $^1O_2$ to form the non-fluorescent 9,10-endoperoxide with a very high rate constant ($2 \times 10^7 - 9 \times 10^8\ M^{-1}s^{-1}$) in many organic solvents, as well as water, Scheme 3 [139].

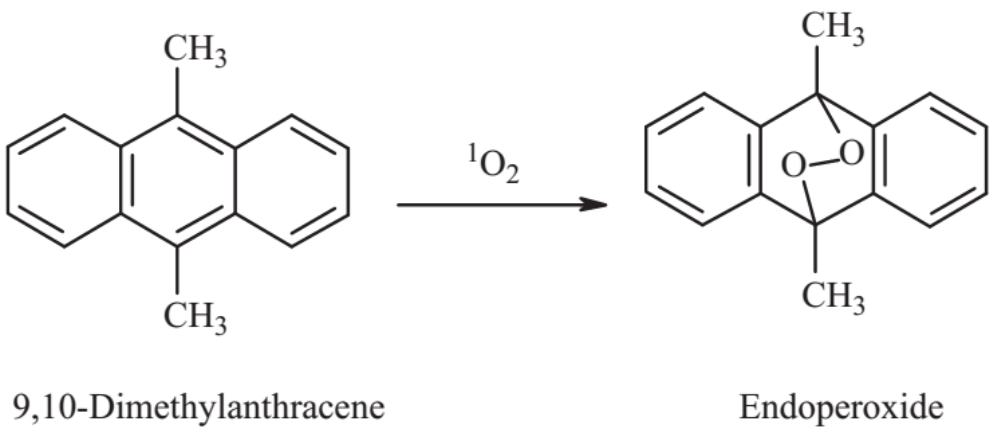

Scheme 3: Reaction of DMA with $^1O_2$ to produce endoperoxide [139].

The endo-peroxide generation was measured using 2 spectroscopic techniques: UV-Vis and fluorescence spectroscopy. Figure 18 shows the UV-Vis spectra of D-NPs along with those of Dye and a control/blank. DMA absorbance at 375 nm decreased from 0.89 to 0.53 (more than 40%) in 80 min of illumination with a green light. In contrast, D-NPs and the blank/control showed practically no decrease in DMA absorbance confirming the absence of any singlet oxygen generation. The fluorescence spectra, Figure 18, show a similar result. The dye alone was able to generate enough singlet oxygen in 80 min to decrease the fluorescence intensity of DMA at 424 nm by more than 35%. The spectra of D-NPs and the blank are similar and show negligible decrease in absorbance and fluorescence after 80 min of excitation. These results prove that our D-NPs photosensitizers don't generate singlet oxygen upon excitation, and therefore act mainly through Type I mechanism in their PDT action.

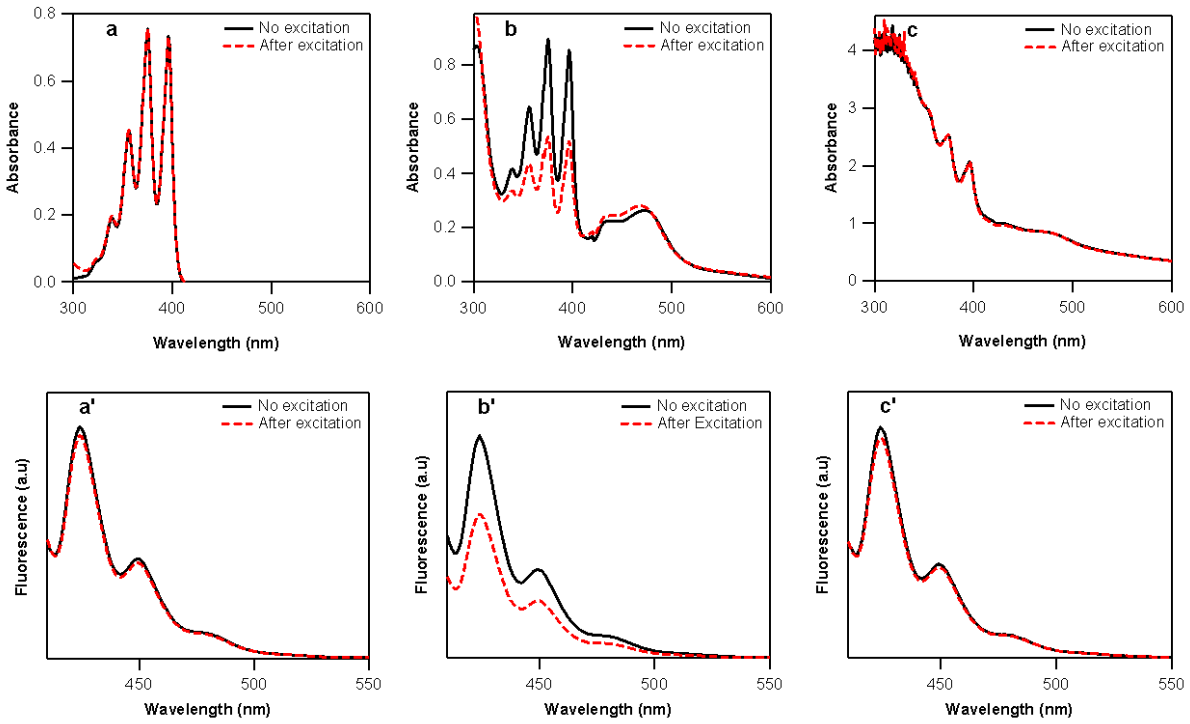

Figure 18: UV-Vis (top) and fluorescence emission spectra (bottom) of DMA before and after 80 min excitation with a green light for the samples a-a' (blanks), b-b' (Dye) and c-c' (D-NPs) in PBS buffer.

After demonstrating the efficiency of D-NPs at generating ROS in solution, we set to assess their efficacy at killing malignant cells upon light excitation. We chose A549 cells, a commonly used lung cancer cell line model, to determine their NPs internalization, in-cell ROS generation and light induced cell death.

The uptake of NPs into A549 cells was assessed using two independent methods: flow cytometry and fluorescence microscopy. In the former, we quantified the uptake of fluorescein isothiocyanate (FITC) labeled C-NPs (FITC-C-NPs) by cells. This enabled us to use fluorescence assays to measure nanoparticle uptake and visualize nanoparticles within cells. As shown in Figure 19, A549 cells incubated with FITC-C-NPs take up the NPs over several hours with no increase in uptake after 16 hours, and therefore all subsequent experiments were performed after at least 16 hours of incubation time.

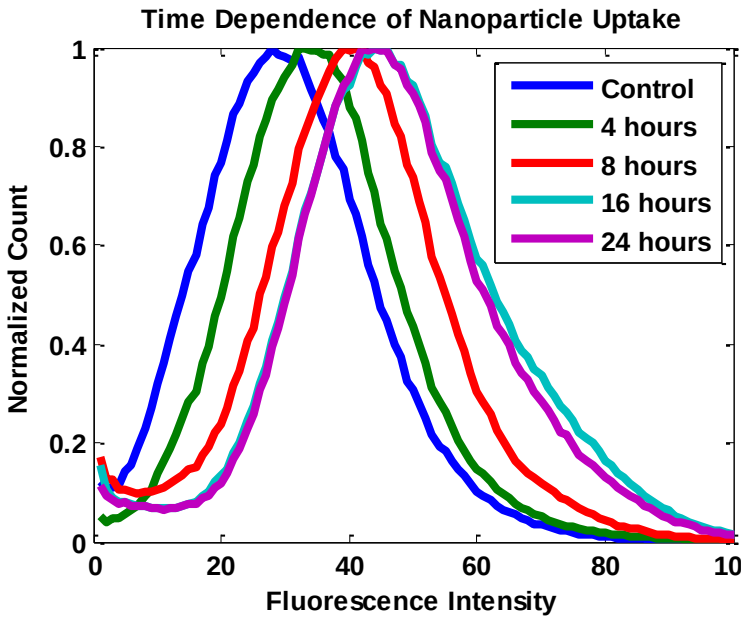

Figure 19: Nanoparticle uptake by A549 cells. A. The histograms shows fluorescence intensity measured via flow cytometry of different time points after treating A549 cells with FITC-C-NPs. Maximum uptake is seen after 16 hours.

However, flow cytometry, while excellent at quantifying overall fluorescence associated with cells, it does not assert whether the NPs are indeed internalized into the cells. Therefore, laser scanning confocal microscopy was performed to ensure the internalization, Figure 20. Calcein blue was used to label the interior of the cells, and we were able to observe that in some cells nanoparticles are clearly within the cytoplasmic volume. We also observed that some nanoparticles appear to be at the periphery of the cells which could be either at the cell membrane or just within that. Some cells also appear empty of any NPs.

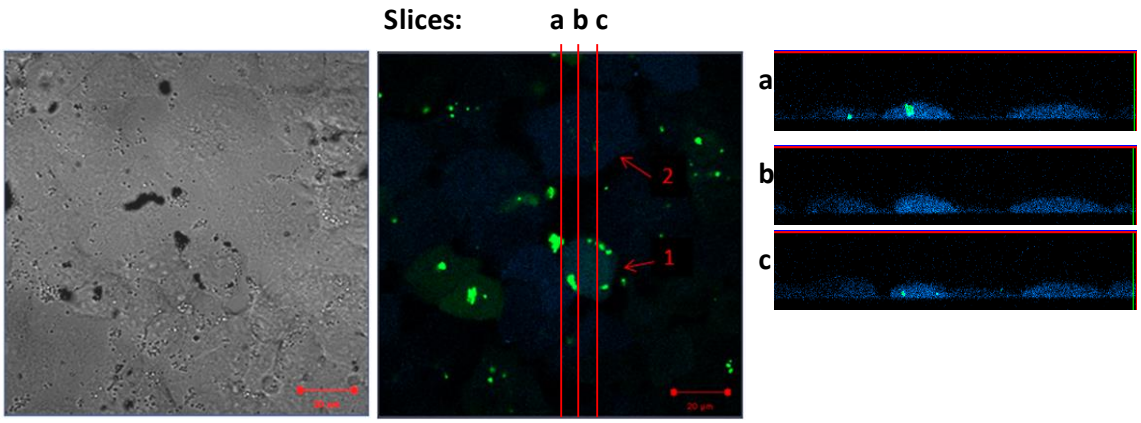

Figure 20: DIC (left) and fluorescence images (middle and right) of A549 cells incubated with FITC-C-NPs. A549 cells are labeled with calcein blue, a cytoplasmic fluorescent dye (blue in middle and right panels). FITC-C-NPs appear green in the fluorescence images and as dark regions in the DIC image. Note the heterogeneity in nanoparticle localization. Cell 1 for example has many nanoparticles on the periphery and internally while cell 2 has little noticeable fluorescence within the cytoplasm. The slices are obtained by acquiring confocal images and show NPs within the cytoplasmic volume of some cells. Scale bar is 20 µm.

After determining nanoparticle uptake, we assessed ROS production by DHE oxidation, Figure 21. D-NPs treated cells, control untreated cells and control C-NPs treated cells were incubated with DHE and directly imaged. A significant increase in ROS production was observed in comparison to the basal level produced in control cells.

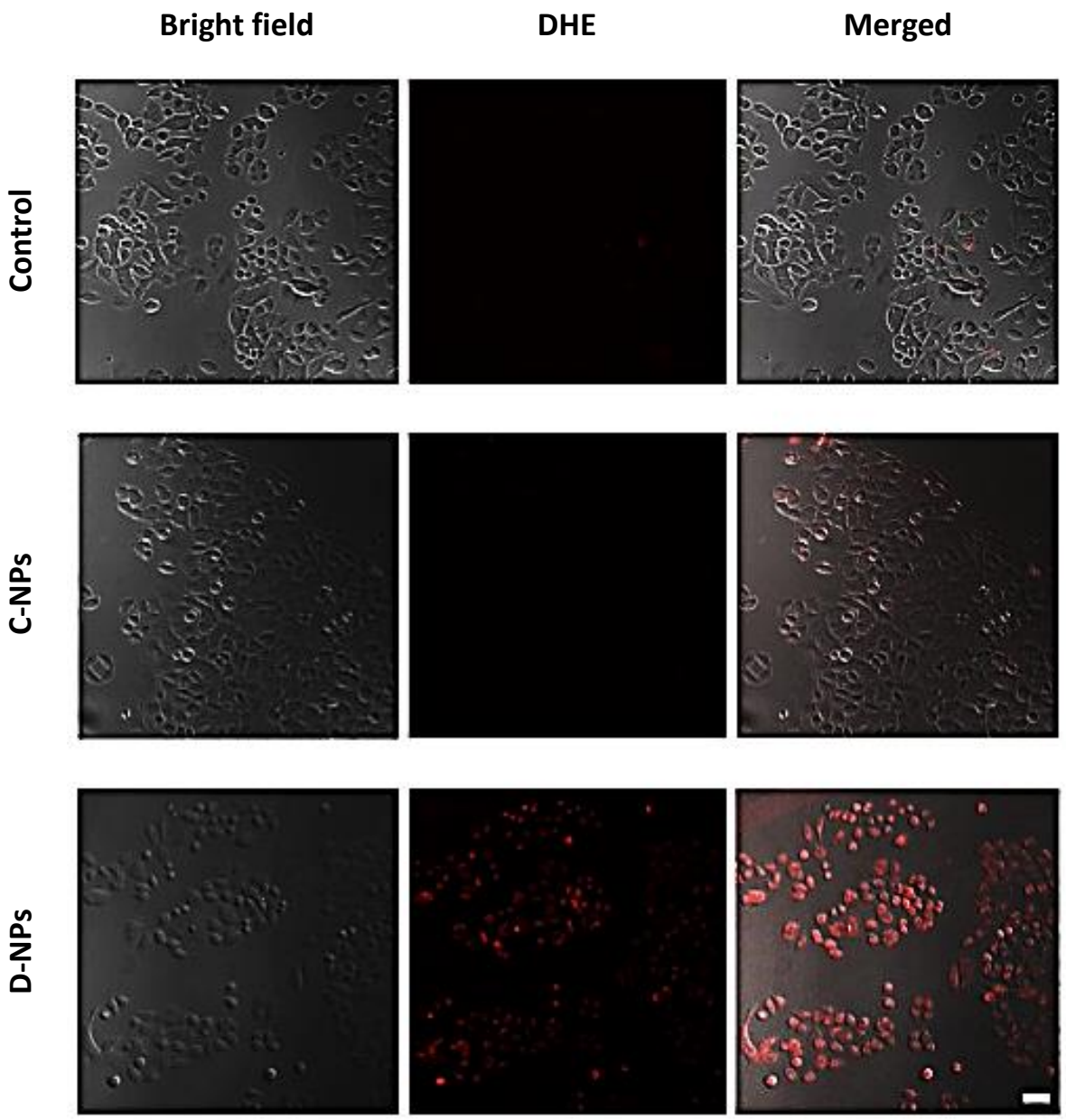

Figure 21: Generation of ROS in A549 D-NPs treated cells. ROS production is significantly increased in D-NPs treated cells. C-NPs treated cells and untreated cells have very low levels of ROS. Images taken in red channel for DHE stain. Scale bar: 5μm.

The observation that D-NPs treated cells showed large ROS production within cells following light excitation suggested that the viability will be compromised. To test this we carried out a microscopy based viability assay. Control untreated cells, control C-NPs treated cells and D-NPs treated cells were all excited with a white light source for 15 minutes and after 24 hours viability was assessed by imaging cells after the addition of calcein green. Living cells with intact cell membranes retain calcein while dead cells lose the dye. Excited

D-NPs treated cells show a large increase in cell death as compared to control cells or to cells treated with C-NPs, Figure 22.

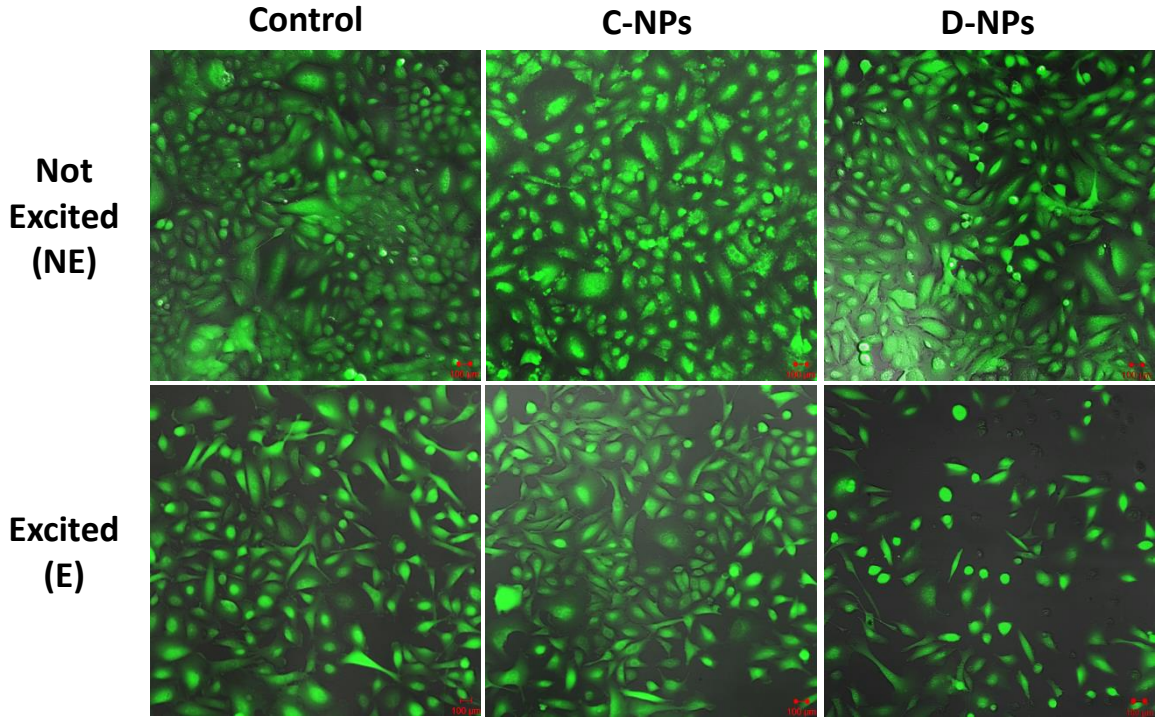

Figure 22: Excitation of A549 D-NPs treated cells with a white light source induces cell death. Top: Images of excited and non-excited A549 D-NPs treated cells and untreated cells were taken 16 hours after excitation. C-NPs treated cells and untreated cells were used as controls. The images are bright field overlaid with calcein green fluorescence. Scale bar: 100μm.

Quantification of cell viability was done by counting the number of living (calcein green containing) and dead cells (non-calcein green containing). Significant numbers of dead cells were observed only with excitation of D-NPs. Cell death was less than 1% of all cells in the control and C-NPs treated cells, while in D-NPs treated one it was between 20 and 40%.

Although our experiment showed a large increase in the death of cells treated with D-NPs compared to controls, the majority of cells remained viable. It is possible that this is due to the fact that different cells took up different amounts of nanoparticles as shown in Figure 20, and/or different cells may also have varying ROS scavenging systems.

CHAPTER VI

CONCLUSION AND FUTURE WORK

In this work, we reported the preparation of core-shell-shell magnetite-silica-titania nanoparticles (Fe_3O_4@SiO_2@TiO_2 NPs) which were stained with a polypyridyl ruthenium dye. The dyed NPs (D-NPs) proved superior to both the naked NPs and the dye alone at generating ROS in solution upon excitation with either white or green light. However, in the ROS generated in solution by the above mentioned NPs no detection of $^1O_2$ was found. We further demonstrated in a proof-of-concept experiment that these nanoparticles are taken up by A549 lung cancer cells. Light excitation of these D-NPs treated A549 cells show an intracellular increase in ROS, and a large increase in cell death after 24 hr.

Future work should focus on enhancing the cellular uptake of the nanocomposites and increasing their efficiency in ROS generation. The former can be achieved by modifying their surface with different functional moieties such as targeting molecules (for example antibodies against certain types of cancer cells). As for ROS generation, exploiting the ruthenium polypyridyl dye for its potential third order nonlinear optical (NLO) process which allows it the simultaneous absorption of two photons. This would allow the excitation with a lower energy laser in the red to NIR light which has a deeper penetration in tissues. Theoretically, the more light that reaches the nanoparticles inside the cells, the more they will be excited, and the more ROS will be generated. On the biology part, future work should also investigate the efficiency of D-NPs *in-vitro* on cells grown at low oxygen levels to verify that the ROS generated, and subsequent cell death, is indeed effective in hypoxic conditions.

REFERENCES

1. Wilson, B.C. *Photodynamic therapy/diagnostics: principles, practice, and advances*. 2010. CRC Press.
2. Triesscheijn, M., et al., *Photodynamic Therapy in Oncology.* The Oncologist, 2006. **11**(9): p. 1034-1044.
3. Dolmans, D.E.J.G.J., D. Fukumura, and R.K. Jain, *Photodynamic therapy for cancer.* Nat Rev Cancer, 2003. **3**(5): p. 380-387.
4. Moor, A.C.E., *Signaling pathways in cell death and survival after photodynamic therapy.* Journal of Photochemistry and Photobiology B: Biology, 2000. **57**(1): p. 1-13.
5. Wyld, L., M.W.R. Reed, and N.J. Brown, *Differential cell death response to photodynamic therapy is dependent on dose and cell type.* Br J Cancer, 2001. **84**(10): p. 1384-1386.
6. Li, W.-T. *Nanoparticles for photodynamic therapy*. 2011. Wiley-VCH Verlag GmbH & Co. KGaA.
7. Brown, S.B., E.A. Brown, and I. Walker, *The present and future role of photodynamic therapy in cancer treatment.* The Lancet Oncology, 2004. **5**(8): p. 497-508.
8. De Rosa, F. and M.V.B. Bentley, *Photodynamic Therapy of Skin Cancers: Sensitizers, Clinical Studies and Future Directives.* Pharmaceutical Research, 2000. **17**(12): p. 1447-1455.
9. Castano, A.P., T.N. Demidova, and M.R. Hamblin, *Mechanisms in photodynamic therapy: part one—photosensitizers, photochemistry and cellular localization.* Photodiagnosis and Photodynamic Therapy, 2004. **1**(4): p. 279-293.
10. Ormond, A. and H. Freeman, *Dye Sensitizers for Photodynamic Therapy.* Materials, 2013. **6**(3): p. 817-840.
11. Macdonald, I.J. and T.J. Dougherty, *Basic principles of photodynamic therapy.* Journal of Porphyrins and Phthalocyanines, 2001. **5**(2): p. 105-129.
12. Hatz, S., J.D. Lambert, and P.R. Ogilby, *Measuring the lifetime of singlet oxygen in a single cell: addressing the issue of cell viability.* Photochem Photobiol Sci, 2007. **6**(10): p. 1106-16.
13. Henderson, B.W. and T.J. Dougherty, *HOW DOES PHOTODYNAMIC THERAPY WORK?* Photochemistry and Photobiology, 1992. **55**(1): p. 145-157.
14. Maiya, B., *Photodynamic Therapy (PDT).* Resonance, 2000. **5**(4): p. 6-18.
15. Bonnett, R. and M.C. Berenbaum, *HPD — A Study of Its Components and Their Properties*, in *Porphyrin Photosensitization*, D. Kessel and T. Dougherty, Editors. 1983, Springer US. p. 241-250.
16. Mironov, A.F., A.N. Nizhnik, and A.Y. Nockel, *Hematoporphyrin derivatives: An oligomeric composition study.* Journal of Photochemistry and Photobiology B: Biology, 1990. **4**(3): p. 297-306.
17. Kessel, D., et al., *Probing the structure and stability of the tumor-localizing derivative of hematoporphyrin by reductive cleavage with LiAlH4.* Cancer Res, 1987. **47**(17): p. 4642-5.
18. Allison, R.R., et al., *Photosensitizers in clinical PDT.* Photodiagnosis and Photodynamic Therapy, 2004. **1**(1): p. 27-42.
19. Bonnett, R., *Photosensitizers of the porphyrin and phthalocyanine series for photodynamic therapy.* Chemical Society Reviews, 1995. **24**(1): p. 19-33.

20. Morgan, A.R., et al., *New photosensitizers for photodynamic therapy: combined effect of metallopurpurin derivatives and light on transplantable bladder tumors.* Cancer Res, 1988. **48**(1): p. 194-8.
21. Moser, J.G. *Attempts to treat malignant melanoma by photodynamic therapy using bacteriopheophorbide ester as the sensitizer*. 1993.
22. Stranadko, E.P., et al. *Photodynamic therapy of cancer: five-year clinical experience*. 1997.
23. Dougherty, T.J., *STUDIES ON THE STRUCTURE OF PORPHYRINS CONTAINED IN PHOTOFRIN® II.* Photochemistry and Photobiology, 1987. **46**(5): p. 569-573.
24. Moan, J. and Q. Peng, *An outline of the history of PDT*, in *Photodynamic Therapy*, T. Patrice, Editor. 2003, The Royal Society of Chemistry. p. 1-18.
25. Stapleton, M. and L.E. Rhodes, *Photosensitizers for photodynamic therapy of cutaneous disease.* J Dermatolog Treat, 2003. **14**(2): p. 107-12.
26. Labbe, R.F. and G. Nishida, *A new method of hemin isolation.* Biochim Biophys Acta, 1957. **26**(2): p. 437.
27. Dougherty, T.J., *PHOTODYNAMIC THERAPY.* Photochemistry and Photobiology, 1993. **58**(6): p. 895-900.
28. Dougherty, T.J., et al., *Photodynamic Therapy.* Journal of the National Cancer Institute, 1998. **90**(12): p. 889-905.
29. Sibata, C.H., et al., *Photodynamic therapy: a new concept in medical treatment.* Braz J Med Biol Res, 2000. **33**(8): p. 869-80.
30. Usuda, J., et al., *Photodynamic therapy (PDT) for lung cancers.* J Thorac Oncol, 2006. **1**(5): p. 489-93.
31. Pushpan, S.K., et al., *Porphyrins in photodynamic therapy - a search for ideal photosensitizers.* Curr Med Chem Anticancer Agents, 2002. **2**(2): p. 187-207.
32. Peng, Q., et al., *5-Aminolevulinic acid-based photodynamic therapy.* Cancer, 1997. **79**(12): p. 2282-2308.
33. Dougherty, T.J., *An Update on Photodynamic Therapy Applications.* Journal of Clinical Laser Medicine & Surgery, 2002. **20**(1): p. 3-7.
34. Batlle, A.M., *Porphyrins, porphyrias, cancer and photodynamic therapy--a model for carcinogenesis.* J Photochem Photobiol B, 1993. **20**(1): p. 5-22.
35. Morton, C.A., et al., *Guidelines for topical photodynamic therapy: report of a workshop of the British Photodermatology Group.* Br J Dermatol, 2002. **146**(4): p. 552-67.
36. Peng, Q., et al., *5-Aminolevulinic acid-based photodynamic therapy: principles and experimental research.* Photochem Photobiol, 1997. **65**(2): p. 235-51.
37. Furre, I.E., et al., *Targeting PBR by hexaminolevulinate-mediated photodynamic therapy induces apoptosis through translocation of apoptosis-inducing factor in human leukemia cells.* Cancer Res, 2005. **65**(23): p. 11051-60.
38. Fingar, V.H., et al., *Analysis of acute vascular damage after photodynamic therapy using benzoporphyrin derivative (BPD).* Br J Cancer, 1999. **79**(11-12): p. 1702-8.
39. Rousset, N., L. Bourre, and S. Thibaud, *Sensitizers in photodynamic therapy*, in *Photodynamic Therapy*, T. Patrice, Editor. 2003, The Royal Society of Chemistry. p. 59-80.
40. Lui, H., et al., *Photodynamic therapy of multiple nonmelanoma skin cancers with verteporfin and red light-emitting diodes: two-year results evaluating tumor response and cosmetic outcomes.* Arch Dermatol, 2004. **140**(1): p. 26-32.
41. Triesscheijn, M., et al., *Outcome of mTHPC mediated photodynamic therapy is primarily determined by the vascular response.* Photochem Photobiol, 2005. **81**(5): p. 1161-7.

42. Dolmans, D.E., D. Fukumura, and R.K. Jain, *Photodynamic therapy for cancer.* Nat Rev Cancer, 2003. **3**(5): p. 380-7.
43. O'Connor, A.E., W.M. Gallagher, and A.T. Byrne, *Porphyrin and nonporphyrin photosensitizers in oncology: preclinical and clinical advances in photodynamic therapy.* Photochem Photobiol, 2009. **85**(5): p. 1053-74.
44. Kobayashi, W., et al., *Photodynamic therapy with mono-L-aspartyl chlorin e6 can cause necrosis of squamous cell carcinoma of tongue: experimental study on an animal model of nude mouse.* Oral Oncol, 2006. **42**(1): p. 46-50.
45. Ali, H. and J.E. van Lier, *Metal complexes as photo- and radiosensitizers.* Chem Rev, 1999. **99**(9): p. 2379-450.
46. Kinsella, T.J., et al., *Preliminary clinical and pharmacologic investigation of photodynamic therapy with the silicon phthalocyanine photosensitizer pc 4 for primary or metastatic cutaneous cancers.* Front Oncol, 2011. **1**: p. 14.
47. Chen, T., et al., *Ruthenium Polypyridyl Complexes That Induce Mitochondria-Mediated Apoptosis in Cancer Cells.* Inorganic Chemistry, 2010. **49**(14): p. 6366-6368.
48. Vos, J.G. and J.M. Kelly, *Ruthenium polypyridyl chemistry; from basic research to applications and back again.* Dalton Transactions, 2006(41): p. 4869-4883.
49. Gill, M.R. and J.A. Thomas, *Ruthenium(ii) polypyridyl complexes and DNA-from structural probes to cellular imaging and therapeutics.* Chemical Society Reviews, 2012. **41**(8): p. 3179-3192.
50. Wachter, E., et al., *Light-activated ruthenium complexes photobind DNA and are cytotoxic in the photodynamic therapy window.* Chemical Communications, 2012. **48**(77): p. 9649-9651.
51. Swavey, S. and K.J. Brewer, *Visible Light Induced Photocleavage of DNA by a Mixed-Metal Supramolecular Complex: [{(bpy)2Ru(dpp)}2RhCl2]5+.* Inorganic Chemistry, 2002. **41**(24): p. 6196-6198.
52. Mari, C., et al., *DNA intercalating Ru(II) polypyridyl complexes as effective photosensitizers in photodynamic therapy.* Chemistry, 2014. **20**(44): p. 14421-36.
53. Liu, Y., et al., *Ru(II) Complexes of New Tridentate Ligands: Unexpected High Yield of Sensitized 1O2.* Inorganic Chemistry, 2008. **48**(1): p. 375-385.
54. Kelly, J.M., et al., *Ruthenium polypyridyl complexes; their interaction with DNA and their role as sensitizers for its photocleavage.* J. Chem. Soc., Chem. Commun., 1987(24): p. 1821-3.
55. Zeglis, B.M. and J.K. Barton, *Binding of Ru(bpy) 2(eilatin) 2+ to Matched and Mismatched DNA.* Inorganic Chemistry, 2008. **47**(14): p. 6452-6457.
56. Tan, C., et al., *Synthesis, structural characteristics, DNA binding properties and cytotoxicity studies of a series of Ru(III) complexes.* Journal of Inorganic Biochemistry, 2008. **102**(8): p. 1644-1653.
57. Corral, E., et al., *Ruthenium polypyridyl complexes and their modes of interaction with DNA: Is there a correlation between these interactions and the antitumor activity of the compounds?* JBIC Journal of Biological Inorganic Chemistry, 2009. **14**(3): p. 439-448.
58. Boerner, L.J.K. and J.M. Zaleski, *Metal complex–DNA interactions: from transcription inhibition to photoactivated cleavage.* Current Opinion in Chemical Biology, 2005. **9**(2): p. 135-144.
59. Barton, J.K., A. Danishefsky, and J. Goldberg, *Tris(phenanthroline)ruthenium(II): stereoselectivity in binding to DNA.* Journal of the American Chemical Society, 1984. **106**(7): p. 2172-2176.

60. Zayat, L., et al., *A New Inorganic Photolabile Protecting Group for Highly Efficient Visible Light GABA Uncaging.* ChemBioChem, 2007. **8**(17): p. 2035-2038.
61. Salierno, M., C. Fameli, and R. Etchenique, *Caged Amino Acids for Visible-Light Photodelivery.* European Journal of Inorganic Chemistry, 2008. **2008**(7): p. 1125-1128.
62. Sun, Y., et al., *Efficient DNA photocleavage by [Ru(bpy)2(dppn)]2+ with visible light.* Chemical Communications, 2010. **46**(14): p. 2426-2428.
63. Goldbach, R.E., et al., *N-Acetylmethionine and Biotin as Photocleavable Protective Groups for Ruthenium Polypyridyl Complexes.* Chemistry – A European Journal, 2011. **17**(36): p. 9924-9929.
64. Wachter, E., et al., *Light-activated ruthenium complexes photobind DNA and are cytotoxic in the photodynamic therapy window.* Chem Commun (Camb), 2012. **48**(77): p. 9649-51.
65. Sgambellone, M.A., et al., *Cellular Toxicity Induced by the Photorelease of a Caged Bioactive Molecule: Design of a Potential Dual-Action Ru(II) Complex.* Journal of the American Chemical Society, 2013. **135**(30): p. 11274-11282.
66. Zhou, Q.-X., et al., *A New Heteroleptic Ruthenium(II) Polypyridyl Complex with Long-Wavelength Absorption and High Singlet-Oxygen Quantum Yield.* Chem. - Eur. J., 2010. **16**(10): p. 3157-3165, S3157/1-S3157/11.
67. Zhang, J.X., et al., *Two-photon induced luminescence, singlet oxygen generation, cellular uptake and photocytotoxic properties of amphiphilic Ru(II) polypyridyl-porphyrin conjugates as potential bifunctional photodynamic therapeutic agents.* Org. Biomol. Chem., 2011. **9**(17): p. 6004-6010.
68. Pernot, M., et al., *Systems biology approach for in vivo photodynamic therapy optimization of ruthenium-porphyrin compounds.* Journal of Photochemistry and Photobiology B: Biology, 2012. **117**(0): p. 80-89.
69. Ke, H., et al., *Synthesis, singlet-oxygen photogeneration, two-photon absorption, photo-induced DNA cleavage and cytotoxic properties of an amphiphilic β-Schiff-base linked Ru(II) polypyridyl-porphyrin conjugate.* J. Lumin., 2014. **154**: p. 356-361.
70. Zhang, J.-X., et al., *Comparative Studies of the Cellular Uptake, Subcellular Localization, and Cytotoxic and Phototoxic Antitumor Properties of Ruthenium(II)–Porphyrin Conjugates with Different Linkers.* Bioconjugate Chemistry, 2012. **23**(8): p. 1623-1638.
71. Rani-Beeram, S., et al., *A Fluorinated Ruthenium Porphyrin as a Potential Photodynamic Therapy Agent: Synthesis, Characterization, DNA Binding, and Melanoma Cell Studies.* Inorganic Chemistry, 2008. **47**(23): p. 11278-11283.
72. Onuki, J., et al., *Supramolecular Cationic Tetraruthenated Porphyrin Induces Single-Strand Breaks and 8-Oxo-7,8-dihydro-2′-deoxyguanosine Formation in DNA in the Presence of Light.* Photochemistry and Photobiology, 1996. **63**(3): p. 272-277.
73. Narra, M., P. Elliott, and S. Swavey, *Synthesis, characterization and DNA interactions of 5,15-(4-pyridyl)-10,20-(pentafluorophenyl)porphyrin coordinated to two [Ru(bipy)2Cl]+ groups.* Inorganica Chimica Acta, 2006. **359**(7): p. 2256-2262.
74. Gianferrara, T., et al., *Ruthenium−Porphyrin Conjugates with Cytotoxic and Phototoxic Antitumor Activity.* Journal of Medicinal Chemistry, 2010. **53**(12): p. 4678-4690.
75. Davia, K., et al., *A porphyrin–ruthenium photosensitizer as a potential photodynamic therapy agent.* Inorganic Chemistry Communications, 2008. **11**(5): p. 584-586.
76. Schmitt, F., et al., *Ruthenium Porphyrin Compounds for Photodynamic Therapy of Cancer.* Journal of Medicinal Chemistry, 2008. **51**(6): p. 1811-1816.

77. Poon, C.T., et al., *An amphiphilic ruthenium(II)-polypyridyl appended porphyrin as potential bifunctional two-photon tumor-imaging and photodynamic therapeutic agent.* J Inorg Biochem, 2010. **104**(1): p. 62-70.
78. Charlesworth, P., et al., *The photophysical properties of a ruthenium-substituted phthalocyanine.* Journal of Photochemistry and Photobiology B: Biology, 1994. **26**(3): p. 277-282.
79. Carneiro, Z.A., et al., *Photocytotoxic activity of a nitrosyl phthalocyanine ruthenium complex — A system capable of producing nitric oxide and singlet oxygen.* Journal of Inorganic Biochemistry, 2011. **105**(8): p. 1035-1043.
80. Zhou, J., et al., *Synthesis and characterization of the monomer ruthenium complex of hypocrellin B.* Bioorganic & Medicinal Chemistry Letters, 2005. **15**(12): p. 3067-3070.
81. Lincoln, R., et al., *Exploitation of Long-Lived 3IL Excited States for Metal–Organic Photodynamic Therapy: Verification in a Metastatic Melanoma Model.* Journal of the American Chemical Society, 2013. **135**(45): p. 17161-17175.
82. Lemercier, G., et al., *3MLCT excited states in Ru(II) complexes: Reactivity and related two-photon absorption applications in the near-infrared spectral range.* Comptes Rendus Chimie, 2008. **11**(6–7): p. 709-715.
83. Brown, S.B., E.A. Brown, and I. Walker, *The present and future role of photodynamic therapy in cancer treatment.* The Lancet Oncology. **5**(8): p. 497-508.
84. Bechet, D., et al., *Nanoparticles as vehicles for delivery of photodynamic therapy agents.* Trends in Biotechnology. **26**(11): p. 612-621.
85. Jori, G., *Tumour photosensitizers: approaches to enhance the selectivity and efficiency of photodynamic therapy.* Journal of Photochemistry and Photobiology B: Biology, 1996. **36**(2): p. 87-93.
86. Solban, N., I. Rizvi, and T. Hasan, *Targeted photodynamic therapy.* Lasers in Surgery and Medicine, 2006. **38**(5): p. 522-531.
87. Verma, S., et al., *Strategies for Enhanced Photodynamic Therapy Effects†.* Photochemistry and Photobiology, 2007. **83**(5): p. 996-1005.
88. Chatterjee, D.K., L.S. Fong, and Y. Zhang, *Nanoparticles in photodynamic therapy: An emerging paradigm.* Adv. Drug Delivery Rev., 2008. **60**(15): p. 1627-1637.
89. Iyer, A.K., et al., *Exploiting the enhanced permeability and retention effect for tumor targeting.* Drug Discovery Today, 2006. **11**(17–18): p. 812-818.
90. Zhang, S., et al., *Enhanced photodynamic therapy of mixed phase TiO2(B)/anatase nanofibers for killing of HeLa cells.* Nano Res., 2014. **7**(11): p. 1659-1669.
91. Zi, F.Y., et al., *Recent progress in biomedical applications of titanium dioxide.* Phys. Chem. Chem. Phys., 2013. **15**(14): p. 4844-4858.
92. Fujishima, A.O., J.; Yamashita, T.; Hayakawa, S., *Behavior of Tumor Cells on Photoexcited Semiconductor Surface.* Journal of Photochemistry and Photobiology B: Biology, 1986: p. 45-46.
93. Sakai, H., et al., *Selective Killing of a Single Cancerous T24 Cell with TiO₂ Semiconducting Microelectrode under Irradiation.* Chemistry Letters, 1995. **24**(3): p. 185-186.
94. Cai, R., et al., *Induction of Cytotoxicity by Photoexcited TiO2 Particles.* Cancer Research, 1992. **52**(8): p. 2346-2348.
95. Kubota, Y., et al., *Photokilling of T-24 human bladder cancer cells with titanium dioxide.* Br J Cancer, 1994. **70**(6): p. 1107-1111.
96. Huang, N.-p., et al., *The study of the photokilling effect and mechanism of ultrafine TiO2 particles on U937 cells.* Journal of Photochemistry and Photobiology A: Chemistry, 1997. **108**(2–3): p. 229-233.

97. Xu, M., et al., *Photoexcited TiO2 nanoparticles through •OH-radicals induced malignant cells to necrosis.* Supramolecular Science, 1998. **5**(5–6): p. 449-451.
98. Zhang, A.P. and Y.P. Sun, *Photocatalytic killing effect of TiO2 nanoparticles on Ls-174-t human colon carcinoma cells.* World J Gastroenterol, 2004. **10**(21): p. 3191-3.
99. Lagopati, N., et al., *Photo-induced treatment of breast epithelial cancer cells using nanostructured titanium dioxide solution.* Journal of Photochemistry and Photobiology A: Chemistry, 2010. **214**(2–3): p. 215-223.
100. Wang, C., et al., *Induction of cytotoxicity by photoexcitation of TiO2 can prolong survival in glioma-bearing mice.* Molecular Biology Reports, 2011. **38**(1): p. 523-530.
101. Cai, R., et al., *Induction of cytotoxicity by photoexcited TiO2 particles.* Cancer Res, 1992. **52**(8): p. 2346-8.
102. Xu, J., et al., *Photocatalytic Inactivation Effect of Gold-Doped TiO2 (Au/TiO2) Nanocomposites on Human Colon Carcinoma LoVo Cells.* International Journal of Photoenergy, 2007. **2007**.
103. Thompson, T.L. and J.T. Yates, *Surface Science Studies of the Photoactivation of TiO2New Photochemical Processes.* Chemical Reviews, 2006. **106**(10): p. 4428-4453.
104. Kumar, S.G. and L.G. Devi, *Review on Modified TiO2 Photocatalysis under UV/Visible Light: Selected Results and Related Mechanisms on Interfacial Charge Carrier Transfer Dynamics.* The Journal of Physical Chemistry A, 2011. **115**(46): p. 13211-13241.
105. Liu, G., et al., *Titania-based photocatalysts-crystal growth, doping and heterostructuring.* Journal of Materials Chemistry, 2010. **20**(5): p. 831-843.
106. Roy, P., S. Berger, and P. Schmuki, *TiO2 Nanotubes: Synthesis and Applications.* Angewandte Chemie International Edition, 2011. **50**(13): p. 2904-2939.
107. Ji, P., et al., *Recent advances in visible light-responsive titanium oxide-based photocatalysts.* Research on Chemical Intermediates, 2010. **36**(4): p. 327-347.
108. Fox, M., et al., *The Effect of Dye Density on the Efficiency of Photosensitization of TiO2 Films: Light-Harvesting by Phenothiazine-Labelled Dendritic Ruthenium Complexes.* Molecules, 2009. **14**(10): p. 3851-3867.
109. Youngblood, W.J., et al., *Visible Light Water Splitting Using Dye-Sensitized Oxide Semiconductors.* Accounts of Chemical Research, 2009. **42**(12): p. 1966-1973.
110. Harriman, A., et al., *Metal oxides as heterogeneous catalysts for oxygen evolution under photochemical conditions.* Journal of the Chemical Society, Faraday Transactions 1: Physical Chemistry in Condensed Phases, 1988. **84**(8): p. 2795-2806.
111. Amouyal, E., *Photochemical production of hydrogen and oxygen from water: A review and state of the art.* Solar Energy Materials and Solar Cells, 1995. **38**(1–4): p. 249-276.
112. Wood, P.M., *The potential diagram for oxygen at pH 7.* Biochemical Journal, 1988. **253**(1): p. 287-289.
113. Janczyk, A., et al., *Photocytotoxicity of platinum(IV)-chloride surface modified TiO2 irradiated with visible light against murine macrophages.* J. Photochem. Photobiol., B, 2008. **92**(1): p. 54-58.
114. Janczyk, A., et al., *Photodynamic activity of platinum(IV) chloride surface-modified TiO2 irradiated with visible light.* Free Radical Biol. Med., 2008. **44**(6): p. 1120-1130.
115. Lei, W., et al., *Photodynamic activity of ascorbic acid-modified TiO2 nanoparticles upon visible illumination (>550 nm).* Chem. Lett., 2009. **38**(12): p. 1138-1139.
116. Tokuoka, Y., et al., *Anticancer Effect of Dye-sensitized TiO₂ Nanocrystals by Polychromatic Visible Light Irradiation.* Chemistry Letters, 2006. **35**(5): p. 496-497.

117. Lopez, T., et al., *Study of the stabilization of zinc phthalocyanine in sol-gel TiO2 for photodynamic therapy applications.* Nanomedicine : nanotechnology, biology, and medicine, 2010. **6**(6): p. 777-785.
118. Pang, S.C., S.Y. Kho, and S.F. Chin, *Fabrication of magnetite/silica/titania core-shell nanoparticles.* J. Nanomater., 2012: p. 427310, 6 pp.
119. Younes, A.H. and T.H. Ghaddar, *Synthesis and Photophysical Properties of Ruthenium-Based Dendrimers and Their Use in Dye Sensitized Solar Cells.* Inorganic Chemistry, 2008. **47**(8): p. 3408-3414.
120. Ng, M., et al., *Highly adsorptive and regenerative magnetic TiO2 for natural organic matter (NOM) removal in water.* Chem. Eng. J. (Amsterdam, Neth.), 2014. **246**: p. 196-203.
121. Xue, C., et al., *High photocatalytic activity of Fe3O4-SiO2-TiO2 functional particles with core-shell structure.* J. Nanomater., 2013: p. 762423, 9 pp.
122. Wu, S.-H., et al., *Cobalt(II) phthalocyanine-sensitized hollow Fe3O4@SiO2@TiO2 hierarchical nanostructures: Fabrication and enhanced photocatalytic properties.* Appl. Surf. Sci., 2013. **287**: p. 389-396.
123. Lucas, M.S., et al., *Photocatalytic degradation of Reactive Black 5 with TiO2-coated magnetic nanoparticles.* Catal. Today, 2013. **209**: p. 116-121.
124. Joo, J., et al., *Magnetically recoverable hybrid TiO2 nanocrystal clusters with enhanced photocatalytic activity.* Mater. Lett., 2013. **93**: p. 141-144.
125. Wang, R., et al., *Preparation and photocatalytic activity of magnetic Fe3O4/SiO2/TiO2 composites.* Adv. Mater. Sci. Eng., 2012: p. 409379, 8 pp.
126. Fan, Y., et al., *Synthesis and properties of Fe3O4/SiO2/TiO2 nanocomposites by hydrothermal synthetic method.* Mater. Sci. Semicond. Process., 2012. **15**(5): p. 582-585.
127. Costa, A.L., et al., *Synthesis of nanostructured magnetic photocatalyst by colloidal approach and spray-drying technique.* J. Colloid Interface Sci., 2012. **388**(1): p. 31-39.
128. Xu, X., et al., *Degradation of glyphosate in soil photocatalyzed by Fe3O4/SiO2/TiO2 under solar light.* Int. J. Environ. Res. Public Health, 2011. **8**: p. 1258-1270.
129. Ye, M., et al., *Magnetically recoverable core-shell nanocomposites with enhanced photocatalytic activity.* Chem. - Eur. J., 2010. **16**(21): p. 6243-6250.
130. Chen, J., et al., *Synthesis and characterization of magnetic nanocomposites with Fe3O4 core.* J. Phys.: Conf. Ser., 2009. **152**: p. No pp. given.
131. Truillet, C., et al., *Bifunctional polypyridyl-Ru(II) complex grafted onto gadolinium-based nanoparticles for MR-imaging and photodynamic therapy.* Dalton Trans, 2013. **42**(34): p. 12410-20.
132. Lin, C.-L., C.-F. Lee, and W.-Y. Chiu, *Preparation and properties of poly(acrylic acid) oligomer stabilized superparamagnetic ferrofluid.* Journal of Colloid and Interface Science, 2005. **291**(2): p. 411-420.
133. Ravikumar, C. and R. Bandyopadhyaya, *Mechanistic Study on Magnetite Nanoparticle Formation by Thermal Decomposition and Coprecipitation Routes.* The Journal of Physical Chemistry C, 2011. **115**(5): p. 1380-1387.
134. Stöber, W., A. Fink, and E. Bohn, *Controlled growth of monodisperse silica spheres in the micron size range.* Journal of Colloid and Interface Science, 1968. **26**(1): p. 62-69.
135. Krimm, S., *The infrared spectra of complex molecules, Vol. 1 (3rd ed.), L. J. Bellamy, Halsted Press, a division of John Wiley & Sons, Inc., New York, 1975, 433 pp. $24.00.* Journal of Polymer Science: Polymer Letters Edition, 1976. **14**(2): p. 121-121.

136. Moore, R.G.C., et al., *Room-temperature single-electron tunnelling in surfactant stabilised iron oxide nanoparticles.* Physica E: Low-dimensional Systems and Nanostructures, 2001. **9**(2): p. 253-261.
137. Li, W. and T. Zeng, *Preparation of TiO₂ Anatase Nanocrystals by TiCl₄ Hydrolysis with Additive H₂SO₄*. PLoS ONE, 2011. **6**(6): p. e21082.
138. Wahajuddin and S. Arora, *Superparamagnetic iron oxide nanoparticles: magnetic nanoplatforms as drug carriers.* Int J Nanomedicine, 2012. **7**: p. 3445-71.
139. Gomes, A., E. Fernandes, and J.L.F.C. Lima, *Fluorescence probes used for detection of reactive oxygen species.* Journal of Biochemical and Biophysical Methods, 2005. **65**(2–3): p. 45-80.